https://doi.org/10.5194/acp-2019-1025
Preprint. Discussion started: 8 January 2020
© Author(s) 2020. CC BY 4.0 License.

Atmospheric Chemistry and Physics Discussions

Exploring wintertime regional haze in Northeast China: role of coal and biomass burning

Jian Zhang[1], Lei Liu[1], Liang Xu[1], Qiuhan Lin[1], Hujia Zhao[2], Zhibin Wang[3], Song Guo[4], Min Hu[4], Zongbo Shi[5], Dantong Liu[1], Dao Huang[1], and Weijun Li[1] *

[1]Department of Atmospheric Sciences, School of Earth Sciences, Zhejiang University, Hangzhou, 310027, China

[2]Institute of Atmospheric Environment, China Meteorological Administration, Shenyang, 110016, China

[3]Research Center for Air Pollution and Health, College of Environmental and Resource Sciences, Zhejiang University, Hangzhou, 310058, China

[4]State Key Joint Laboratory of Environmental Simulation and Pollution Control, College of Environmental Sciences and Engineering, Peking University, Beijing, 100871, China

[5]School of Geography, Earth and Environmental Sciences, University of Birmingham, Birmingham, B15 2TT, UK

[*]Corresponding Email: liweijun@zju.edu.cn (W. J. Li)

https://doi.org/10.5194/acp-2019-1025
Preprint. Discussion started: 8 January 2020
© Author(s) 2020. CC BY 4.0 License.

Atmospheric Chemistry and Physics Discussions

Abstract

As one of the intense anthropogenic emission regions across the relatively high latitude (> 40°N) areas on the Earth, Northeast China faces serious problem on regional haze during long winter with half a year. Aerosols in polluted haze in Northeast China are poorly understood compared with the haze in other regions of China such as North China Plain. Here, we for the first time integrated bulk chemical measurements with single particle analysis from transmission electron microscopy (TEM), nanoscale secondary ion mass spectrometer (NanoSIMS), and atomic force microscopy (AFM) to obtain morphology, size, composition, aging process, and sources of aerosol particles collected during two contrasting regional haze events (Haze-I and Haze-II) at an urban site and a mountain site in Northeast China, and further investigated the causes of regional haze formation. Haze-I evolved from moderate (average $PM_{2.5}$: 76-108 $\mu g/m^3$) to heavy pollution (151-154 $\mu g/m^3$), with the dominant $PM_{2.5}$ component changing from organic matter (OM) (39-45 $\mu g/m^3$) to secondary inorganic ions (94-101 $\mu g/m^3$). Similarly, TEM observations showed that S-OM particles elevated from 29% to 60% by number at urban site and 64% to 74% at mountain site and 75-96% of Haze-I particles included primary OM. Change of wind direction induced that Haze-I rapidly turned into Haze-II (185-223 $\mu g/m^3$) with the predominant OM (98-133 $\mu g/m^3$) and unexpectedly high K^+ (3.8 $\mu g/m^3$). TEM also showed that K-OM particles increased from 4-5% by number to 50-52%. Our study revealed a contrasting formation mechanism of these two haze events: Haze-I was induced by accumulation of primary OM emitted from residential coal burning and further deteriorated by secondary aerosol formation via heterogeneous reactions; Haze-II was caused by long-range transport of agricultural biomass burning emissions. Moreover, we found that 75-97% of haze particles contained tarballs, but only 4-23% contained black carbon and its concentrations were low at 2.7-4.3 $\mu g/m^3$. The results highlight that abundant tarballs are important light-absorbing brown carbon in Northeast China during winter haze and further considered in climate models.

https://doi.org/10.5194/acp-2019-1025
Preprint. Discussion started: 8 January 2020
© Author(s) 2020. CC BY 4.0 License.

Atmospheric Chemistry and Physics Discussions

1. Introduction

Haze pollution is mainly caused by high levels of fine particulate matter ($PM_{2.5}$) and it has widely spread over the globe such as Mexico city (Adachi and Buseck, 2008), Paris, France (Fortems‐Cheiney et al., 2016), North India (Chowdhury et al., 2019), North China (Huang et al., 2014), and the Arctic (Frossard et al., 2011). In the past twenty years, regional haze episodes with high concentrations of $PM_{2.5}$ have frequently occurred in China following rapid economic development. Various studies on regional haze in China have been conducted by many scientists (e.g., Bennartz et al., 2011; Guo et al., 2014; Li and Shao, 2009; Lin et al., 2017; Liu et al., 2017b; Ren et al., 2016; Shi et al., 2017; Zhang et al., 2018b). Current hot issues on haze pollution concentrate on the formation processes of regional haze in various atmospheric environments and their potential optical and health influences (Chen et al., 2017a; Gao et al., 2017).

Many of these studies reported that haze particles can adversely affect human health, ecological environments, and regional climate (Ding et al., 2016; Huang et al., 2013; Lelieveld et al., 2015; Li et al., 2017a; Liu et al., 2019; Liu et al., 2016; Mahowald et al., 2018; Shi et al., 2019; Xie et al., 2019; Zhang et al., 2013). For example, exposure to high levels of ambient $PM_{2.5}$ cause or contribute to a variety of human diseases (e.g., stroke, ischemic heart disease, chronic obstructive pulmonary disease, and lung cancer) (Chen et al., 2019; Liu et al., 2016) and lead to ~1.3 million premature deaths per year in China (Lelieveld et al., 2015). Abundant anthropogenic metal, ammonium, and phosphorus-containing particles are transported into remote regions of oceans, where they promote plankton growth and further influence ocean ecology (Li et al., 2017a; Mahowald et al., 2018; Shi et al., 2019). High concentrations of fine aerosols suspended in haze layers not only influence regional climate through absorbing (e.g., black carbon (BC) and brown carbon (BrC)) and scattering (e.g., sulfates and nitrates) solar radiation (Huang et al., 2013; Liu et al., 2019; Xie et al., 2019), but also depress the planetary boundary layer development

https://doi.org/10.5194/acp-2019-1025
Preprint. Discussion started: 8 January 2020
© Author(s) 2020. CC BY 4.0 License.

Atmospheric Chemistry and Physics Discussions

(Ding et al., 2016; Li et al., 2017c; Zhang et al., 2013) and reduce crop yields (Tie et al., 2016) in China. Therefore, understanding haze formation mechanisms and sources of haze particles in different regions of China is crucial to provide feasible control strategies for reducing regional $PM_{2.5}$ concentration and protecting ecosystems.

In China, regional heavy hazes frequently occur in the North China Plain (NCP) (Zhao et al., 2013) and Northeast China (Ma et al., 2018) during winter. In the past decades, the regional haze formation mechanisms in the NCP have been intensely investigated (Chen et al., 2017b; Cheng et al., 2016; Li et al., 2015; Liu et al., 2017c; Tao et al., 2014; Tian et al., 2015; Wang et al., 2016; Wang et al., 2019; Wang et al., 2014; Xing et al., 2019; Zheng et al., 2015b; Zhong et al., 2019). Adverse meteorological conditions (e.g., low wind speeds and stable atmospheric boundary layer) can induce preliminary formation of hazes during winter (Zheng et al., 2015b; Zhong et al., 2019). Massive numbers of primary particles from industries, households, and vehicular exhaust emissions (e.g., fly ash, metal, primary organic matter, and soot particles) are the major aerosols in winter hazes (Chen et al., 2017b; Tian et al., 2015; Wang et al., 2019). Rapid production of secondary aerosols (e.g., sulfates, nitrates, and secondary organics) via heterogeneous reactions under high RH mainly elevates haze levels and causes regional hazes (Liu et al., 2017c; Wang et al., 2016; Xing et al., 2019). The two-way feedback between accumulation of air pollutants and depression of the atmospheric boundary layer also aggravate haze pollution (Wang et al., 2014; Zhong et al., 2019). Moreover, regional transport of air pollutants is one of the important factors for the long duration of regional haze (Li et al., 2015; Tao et al., 2014; Zheng et al., 2015b). These studies well revealed formation mechanisms of regional winter hazes in the NCP.

Among different regions or cities in China, the haze formation mechanisms would most likely differ due to different emissions and meteorological conditions (Li et al., 2019; Zhang et al., 2017; Zheng et al., 2015b). The air quality in Northeast China, a region with a long heating period (mid October-mid April), is mainly

https://doi.org/10.5194/acp-2019-1025
Preprint. Discussion started: 8 January 2020
© Author(s) 2020. CC BY 4.0 License.

Atmospheric Chemistry and Physics Discussions

influenced by abundant inefficient combustion activities (e.g., coal and biomass burning in residential stoves and coal burning in small boilers for household heating and cooking) (Yang et al., 2017; Zhang et al., 2017). Extremely high concentrations of organic aerosols have been observed in Northeast China during winter haze that coincide with crop growing and harvest periods (Cao et al., 2017; Chen et al., 2015; Zhang et al., 2017). Because of the influences of the regional haze in winter, annual aerosol optical depth in urban areas was ~3.7 times higher than that in rural areas in Northeast China (Zhao et al., 2018b). In the past five years, some studies have focused on the physicochemical properties of haze particles collected in Northeast China (Cao et al., 2017; Chen et al., 2015; Li et al., 2017b; Miao et al., 2018; Zhang et al., 2017; Zhao et al., 2018b). However, studies on regional haze evolution and haze formation mechanisms in Northeast China are rare. This limited information precludes the comparison of regional hazes in Northeast China with other regions in China. Furthermore, it is difficult to adopt some reasonable regional haze pollution control strategies from the NCP to apply to the air pollution in Northeast China.

Northeast China is only one intense anthropogenic emission region besides Mongolia across the relatively high latitude (> 40°N) areas on the Earth (van Donkelaar et al., 2016). This region is significantly influenced by the Siberian cold high pressure systems in winter. The Siberian anticyclone transports air pollutants from Northeast China to Korea, Japan, and even the Arctic, and further causes large-scale influences in the global climate (Jung et al., 2015; Rodo et al., 2014; Sobhani et al., 2018; Zhang et al., 2016). Therefore, understanding the physicochemical characteristics of anthropogenic fine particles in regional haze and regional haze formation mechanisms over Northeast China has to be considered of the utmost importance.

In this study, we conducted a field experiment in the south part of Northeast China from 31 October to 6 November 2016. Two contrasting regional heavy haze episodes occurred there during the sampling period. We investigated the types and

https://doi.org/10.5194/acp-2019-1025
Preprint. Discussion started: 8 January 2020
© Author(s) 2020. CC BY 4.0 License.

Atmospheric Chemistry and Physics Discussions

mixing states of individual aerosol particles and $PM_{2.5}$ composition during these two episodes. Finally, we elucidated the formation mechanisms of two regional haze events and the main sources of fine haze particles.

2. Experimental Methods

2.1 Sampling sites and sample collections

There are three provincial capital cities (i.e., Shenyang, Changchun, and Harbin) in Northeast China that are surrounded by the Greater Khingan Mountains, the Lesser Khingan Mountains, and the Changbai Mountains (Figure 1a). In this study, we selected an urban site (41.8°N, 123.35°E) and a mountain site (41.92°N, 123.65°E) in Shenyang city (Figure 1b). The urban site is located in the center of Shenyang city. The mountain site on top of Qipan Mountain (224 m) is located ~30 km northeast of the urban site (Figure 1b). There are only a few villages around Qipan Mountain, so its air quality well represents the regional transport in the south part of Northeast China.

The $PM_{2.5}$ samples were collected on 90 mm quartz filters (Whatman, UK) using two medium volume samplers (Wuhan Tianhong Inc., TH-150A, 100 L/min) at the urban and mountain sites. Individual particle samples were collected on transmission electron microscopy (TEM) grids and silicon wafers using two DKL-2 samplers (Genstar Inc., 1 L/min) equipped with a 0.5 mm jet nozzle impactor at two sampling sites. The quartz filters provided mass concentrations and the chemical composition of ambient $PM_{2.5}$. The TEM grids and silicon wafers were used for microscopic observations of individual particles. To better explore the variation of $PM_{2.5}$ composition and individual particles, we collected the daytime (DT, 8:30-20:00 (local time)) $PM_{2.5}$ and nighttime (NT, 20:30-8:00 (next day)) $PM_{2.5}$ as well as individual particle samples four times a day (i.e., 0:00-3:00, 6:00-9:00, 12:00-15:00, and 18:00-21:00). To avoid individual particles overlapping on the substrate, the sampling duration of individual particles was varied from 30 s to 10 min depending on the $PM_{2.5}$ concentrations. After individual particles samples were collected, we immediately

https://doi.org/10.5194/acp-2019-1025
Preprint. Discussion started: 8 January 2020
© Author(s) 2020. CC BY 4.0 License.

Atmospheric Chemistry and Physics Discussions

used a portable optical microscope to check the particle distribution on the substrate, which guaranteed the sample to be suitable for microscopic analyses. After the sampling, the quartz filters were put into a -20 °C refrigerator and the TEM grids and silicon wafers were stored in the dry, clean, and airtight containers until laboratory analyses were performed.

Meteorological data (i.e., wind speed and wind direction, temperature, relative humidity (RH), and pressure) at the urban and mountain sites were simultaneously collected by two automated weather instruments (Kestrel 5500, USA) at five minute intervals.

2.2 $PM_{2.5}$ analyses

The quartz filters are weighed with a high-precision digital balance (Sartorius ME 5-F, 0.001 mg of reading precision) after being equilibrated for 24 h under stable conditions (TP: 20±1 °C; RH: 48±2%) before and after sampling. The $PM_{2.5}$ mass concentrations at the urban and mountain sites are calculated based on the weight difference and sampling volume of each quartz filter.

Each quartz filter collected at two sampling sites can be used to analyze chemical composition (i.e., water-soluble ions, organic carbon (OC), and elemental carbon (EC)) of $PM_{2.5}$. In this study, we use an ion chromatography system (Dionex ICs-90, USA) to obtain mass concentrations of water-soluble ions (i.e., Ca^{2+}, Mg^{2+}, K^+, Na^+, NH_4^+, NO_3^-, SO_4^{2-}, Cl^-, and F^-) and an OC/EC analyzer (Sunset Laboratory Inc., USA) to obtain mass concentrations of OC and EC. Concentrations of organic matter (OM) were further calculated through multiplying OC concentrations by a factor of 1.4 reported by Guinot et al. (2007). The experimental details about water-soluble ions analysis and OC/EC analysis have been provided in our previous study (Zhang et al., 2017).

2.3 TEM/EDS analysis

https://doi.org/10.5194/acp-2019-1025
Preprint. Discussion started: 8 January 2020
© Author(s) 2020. CC BY 4.0 License.

Atmospheric Chemistry and Physics Discussions

Individual particles on TEM grids (copper (Cu) grid covered by a carbon (C) reinforcement substrate) are examined using TEM combined with energy-dispersive X-ray spectrometry (EDS) (JEOL, JEM-2100). TEM observation provide the morphology of individual particles and the mixing states of different aerosol components in individual particles on the substrate. EDS determines the elemental composition of individual particles. EDS spectra of individual particles are collected within a maximum time of 30 s to minimize potential X-ray damage and ensure sufficient intensity during EDS analysis. Cu cannot be analyzed for individual particles because the TEM grids are made of Cu. In addition, the C content in EDS spectra of individual particles may be overestimated due to the substrate's contribution.

Individual particles are unevenly distributed on TEM grids, with coarser particles in the center of sampling spot and finer particles on the periphery. Therefore, to guarantee that the analyzed particles are representative, five areas are selected from the sampling center to periphery on each TEM grid. After a labor-intensive operation, a total of 3,630 particles at the urban site and 4,281 particles at the mountain site with diameter < 2.5 μm were analyzed by TEM/EDS.

The area, perimeter, and equivalent circle diameter (ECD) of individual particles in TEM images are manually or automatically obtained through an image analysis software (iTEM, Olympus soft imaging solutions GmbH, Germany).

2.4 NanoSIMS analysis

Based on TEM/EDS analysis, a representative individual particle sample is selected for nanoscale secondary ion mass spectrometer (NanoSIMS, 50L, CAMECA Instruments, Geneviers, France) analysis. In this work, signal intensity mapping of $^{12}C^{14}N^-$, $^{12}C^-$, $^{16}O^-$, and $^{32}S^-$ ions are obtained after the Cs^+ primary ion beam ionizes the atoms of particle surface. Ion signal intensity mapping of individual particles with nanometer resolution clearly shows ion distribution in particles. Strong $^{12}C^{14}N^-$ and $^{12}C^-$ signals imply OM in individual particles and eliminate the contribution of C

https://doi.org/10.5194/acp-2019-1025
Preprint. Discussion started: 8 January 2020
© Author(s) 2020. CC BY 4.0 License.

substrate on TEM grids (Chi et al., 2015).

2.5 AFM analysis

The surface structure of individual particles collected on silicon wafers are investigated using atomic force microscopy (AFM, Dimension Icon, USA) with a digital nanoscope IIIa in the tapping mode. AFM observations in the tapping mode produce 3-D images of individual particles. The tapping AFM is equipped with a cantilever and a conical tip with a 10 nm radius.

Based on the preliminary observations from TEM, we select three typical samples collected during the clean day, Haze-I event, and Haze-II event for the AFM analysis (The naming details for haze events in Section 3.1). To obtain the 3-D morphology of more particles on the basis of keeping images clear, 10 × 10 μm^2 of scanning range and 0.5-0.8 Hz of scanning rate are selected. 57 particles during the clean day and Haze-I and 29 particles during the Haze-II were carefully analyzed. After obtaining AFM images of individual particles, we use the NanoScope Analysis software to automatically obtain the bearing area (A) and bearing volume (V) of each analyzed particle. The ECD and equivalent sphere diameter (ESD) of individual particles are further calculated according to the following two formulas.

$$A = \frac{4}{3}\pi r^2 = \frac{\pi d^2}{3} \rightarrow d = \sqrt{\frac{3A}{\pi}} \quad (1)$$

$$V = \frac{4}{3}\pi r^3 = \frac{4}{3} \times \frac{\pi D^3}{8} \rightarrow D = \sqrt[3]{\frac{6V}{\pi}} \quad (2)$$

Where d is ECD; D is ESD.

The linear correlations between ECD and ESD and typical AFM images of individual particles (clean day & Haze-I: D=0.5861×d; Haze-II: D=0.4040×d) are shown in Figures S1a-b. Through the above two linear correlations, we can obtain the ESD of each individual particle analyzed by iTEM software.

https://doi.org/10.5194/acp-2019-1025
Preprint. Discussion started: 8 January 2020
© Author(s) 2020. CC BY 4.0 License.

Atmospheric Chemistry and Physics Discussions

3. Results

3.1 Composition of fine particles and meteorology

Regional haze pollution was observed in Northeast China during the sampling period from 31 October to 5 November 2016 (Figure S2). Based on the variation of $PM_{2.5}$ mass concentration and visibility at the urban and mountain sites, clean day (31 DT October, $PM_{2.5} < 75$ μg/m^3 and visibility > 10 km) and haze days (31 NT October-5 NT November, $PM_{2.5} \geq 75$ μg/m^3 and visibility < 10 km) were identified (Figure 2a). In general, we determined two regional haze events: 31 NT October-4 DT November (Haze-I) and 4 NT-5 NT November (Haze-II), based on the different prevailing wind directions (Haze-I: Southerly; Haze-II: Northerly) (Figures S3a-b) and air mass backward trajectories (Figure S4).

To understand haze evolution, we divided Haze-I event into a moderate haze stage (31 NT October-3 NT November) with 75 μg/m^3 ≤ $PM_{2.5}$ < 150 μg/m^3 and a heavy haze stage (4 DT November) with $PM_{2.5} \geq 150$ μg/m^3 (Figure 2a). Figure 2a shows that the average mass concentrations of $PM_{2.5}$ increased from 69 μg/m^3 to 108 μg/m^3 at the urban site and from 25 μg/m^3 to 76 μg/m^3 at the mountain site from the clean day to the moderate Haze-I event. Compared with northerly winds with ~1.4 m/s and ~38% of RH on the clean day, the wind directions were from the southerly with 0.7 m/s at the urban site and 3.0 m/s at the mountain site; RH varied from 39% to 67% during the moderate Haze-I event (Figures S3a-d). Here the moderate Haze-I event is considered as a general haze pollution that frequently occurs in Northeast China during winter (Zhang et al., 2017). During the moderate Haze-I event, the average mass concentrations of OM, EC, and secondary inorganic ions (i.e., SO_4^{2-}, NO_3^-, and NH_4^+) in $PM_{2.5}$ were 45 μg/m^3, 4.3 μg/m^3, and 24 μg/m^3 at the urban site and 39 μg/m^3, 2.7 μg/m^3, and 20 μg/m^3 at the mountain site, respectively (Figures 2b-c). Following $PM_{2.5}$ concentration exceeding 150 μg/m^3, the moderate Haze-I event evolved into the heavy Haze-I event (Figure 2a). During the heavy Haze-I event, mass concentrations of $PM_{2.5}$ were 154 μg/m^3 at the urban site and 151 μg/m^3 at the

https://doi.org/10.5194/acp-2019-1025
Preprint. Discussion started: 8 January 2020
© Author(s) 2020. CC BY 4.0 License.

Atmospheric Chemistry and Physics Discussions

mountain site (Figure 2a). RH remained high at 73-80% at the urban and mountain sites during the heavy Haze-I event (Figures S3c-d). Figures 2b-c show that the average concentrations of OM and EC were fairly constant at 39-45 μg/m^3 and 2.7-4.3 μg/m^3 from the moderate Haze-I to the heavy Haze-I event. In contrast, secondary inorganic ions rapidly increased from 20-24 μg/m^3 to 94-101 μg/m^3 in the DT of 4 November (Figures 2b-c). Therefore, the variation of chemical composition of $PM_{2.5}$ clearly reflected the general haze evolution from moderate to heavy in Northeast China.

With the prevailing wind changing from southerly with ~0.8 m/s to northerly with ~3.9 m/s (Figures S3a-b), the Haze-I event turned into the Haze-II event. The average $PM_{2.5}$ concentrations remained at high levels and reached 223 μg/m^3 at the urban site and 185 μg/m^3 at the mountain site (Figure 2a). RH were consistently high in the range of 65-87% during the Haze-II event (Figures S3c-d). In addition, we noticed that hourly concentrations of $PM_{2.5}$ and CO rapidly climbed from 209 μg/m^3 and 1.3 ppm at 6:00 A.M. to 669 μg/m^3 and 1.9 ppm at 8:00 A.M. on 5 November, respectively (Figures S5a-b). Although $PM_{2.5}$ concentrations during the Haze-II event were close to those of the heavy Haze-I event, we found large differences between aerosol chemistry in these two heavy haze episodes besides the prevailing wind direction (Figures 2a-c). From the heavy Haze-I to the Haze-II events, secondary inorganic ions significantly decreased from 62-66% of the total $PM_{2.5}$ mass (94-101 μg/m^3) to 31-35% (65-70 μg/m^3); but OM markedly increased from 27-30% (42-45 μg/m^3) to 53-60% (98-133 μg/m^3) (Figures 2a-c). In addition, K^+ average concentrations unexpectedly increased from 1.4 μg/m^3 during the heavy Haze-I event to 3.8 μg/m^3 during the Haze-II event (Figures 2b-c). As a result, the difference between $PM_{2.5}$ composition before and after 4 November again proved that there were two different haze episodes under the different prevailing wind directions. These two regional haze episodes might have different formation mechanisms (details in Section 4.1).

3.2 Characteristics of individual haze particles

https://doi.org/10.5194/acp-2019-1025
Preprint. Discussion started: 8 January 2020
© Author(s) 2020. CC BY 4.0 License.

Atmospheric Chemistry and Physics Discussions

296 TEM/EDS did an excellent job of determining the morphology and composition
297 of individual particles as shown in Figures 3a-j. NanoSIMS was used to further
298 identify OM particles through ions ($^{12}C^{14}N^-$, $^{12}C^-$, $^{16}O^-$, and $^{32}S^-$) signal mappings in
299 order to exclude the interfere of C substrate on TEM grids to EDS (Figure 3k). Figure
300 3k shows high $^{12}C^{14}N^-$ and $^{12}C^-$ signals but low $^{32}S^-$ signal, which strongly confirms
301 the OM particle. As a result, six basic types of aerosol components were classified
302 based on their morphology, composition, and ion signal mapping: mineral, OM, soot
303 (also known as EC and BC), fly ash/metal, S-rich, and K-rich (Figures 3a-k).
304 Mineral particles mainly contain O, Si, Al, and Fe elements and present irregular
305 shape (Figures 3a-1 and 3a-2). Mineral particles mainly occurred in the coarse size
306 range (> 1 μm) (Figures S6a-b), and they were often externally mixed with other
307 types of particles (i.e., OM, soot, fly ash/metal, S-rich, and K-rich particles) (Figure
308 3a-1). OM particles are mainly composed of C, O, and Si (Figures 3b-2, 3c-2, and
309 3i-2). OM particles were further classified into spherical OM (Figure 3b-1), domelike
310 OM (Figure 3c-1), and OM coating (Figures 3i-1 and 3j) based on their morphology.
311 TEM observations showed that most OM particles were internally mixed with S-rich
312 (Figure 3f-1), soot (Figure 3g), and K-rich (Figures 3i-1 and 3j) particles. Soot
313 particles mainly include C and O elements and are aggregates of carbonaceous
314 spheres (Figures 3d-1 and 3d-2). Figures S6a-b show that soot particles mainly
315 occurred in the fine size range (< 200 nm). TEM observations showed that a majority
316 of soot particles were internally mixed with S-rich or OM particles, which were
317 classified as soot-S/OM particles (Figure 3g). Fly ash/metal particles with spherical
318 morphology are mainly comprised of O, Si, and metallic elements (e.g., Al, Fe, Mn,
319 and Pb) (Figures 3e-1 and 3e-2). Fly ash/metal particles were mainly in the ultrafine
320 size range (< 100 nm) (Figures S6a-b) and internally mixed with S-rich or OM
321 particles, which were called fly ash/metal-S/OM particles (Figure 3h). S-rich particles
322 are mainly composed of O, S, and N (Figure 3f-2) and formed from the oxidation of
323 SO_2, NO_x, and NH_3. S-rich particles normally represent the mixtures of $(NH_4)_2SO_4$

https://doi.org/10.5194/acp-2019-1025
Preprint. Discussion started: 8 January 2020
© Author(s) 2020. CC BY 4.0 License.

Atmospheric Chemistry and Physics Discussions

and NH_4NO_3 (Li et al., 2016). TEM observations showed that abundant S-rich particles were internally mixed with OM particles, called S-OM particles (Figure 3f-1). K-rich particles mainly contain K, O, S, and N elements (Figure 3i-3). All K-rich particles were internally mixed with OM particles, and were called K-OM particles (Figures 3i-1 and 3j). To compare number fractions of OM particles during the haze evolution, here we considered the particles including OM as OM-containing particles. In the same way, soot-containing and fly ash/metal-containing particles were also defined.

Figure 4 shows the variation of number fractions of different particles types at the urban and mountain sites from the clean day to the Haze-I event and to the Haze-II event. At the urban site, these data show that mineral and S-OM were the major particle types, which accounted for 36% and 23% during the clean day. Subsequently, S-OM, OM, and soot-containing particles became major particle types which accounted for 29%, 18%, and 23% at the urban site during the moderate Haze-I event. During the heavy Haze-I event, S-OM particles dominated at 60% at the urban site (Figure 4). Interestingly, we found that S-OM particles remained at very high frequencies (61-74%) at the mountain site from the clean day to the Haze-I event (Figure 4). Furthermore, the pink frames in Figure 4 show that OM-containing (i.e., S-OM, OM, soot-OM, fly ash/metal-OM, and K-OM) particles accounted for 75-86% at the urban site and 95-96% at the mountain site during the Haze-I event. During the Haze-II event, number fractions of OM-containing particles reached their maximum at 96% at the urban site and 97% at the mountain site (Figure 4). It is noted that K-OM became the predominant particles in the Haze-II event, accounting for 50% at the urban site and 52% at the mountain site (Figure 4). Therefore, individual particle analysis clearly shows large differences of particle types and fractions following the haze evolution, which is consistent with the variation of $PM_{2.5}$ composition described in Section 3.1.

https://doi.org/10.5194/acp-2019-1025
Preprint. Discussion started: 8 January 2020
© Author(s) 2020. CC BY 4.0 License.

Atmospheric Chemistry and Physics Discussions

3.3 Pollutants change following haze evolution and transformation

The analysis of X/EC (e.g., $PM_{2.5}$/EC, OC/EC, SO_4^{2-}/EC, NO_3^-/EC, and K^+/EC) factors not only can exclude the influence of changes in atmospheric boundary layer height on pollutants mass concentrations, but also indicate accumulation (e.g., small changes in X/EC) and secondary formation (e.g., increases of SO_4^{2-}/EC and NO_3^-/EC) of $PM_{2.5}$ during haze evolution (Zhang et al., 2017; Zheng et al., 2015b). Although $PM_{2.5}$ concentrations increased from 69 μg/m^3 to 108 μg/m^3 at the urban site and from 25 μg/m^3 to 76 μg/m^3 at the mountain site from the clean day to the moderate Haze-I event, X/EC factors only displayed minor variations (Figures 5a-b). This result shows that accumulation of air pollutants mainly induced the moderate Haze-I formation. Following formation of the heavy Haze-I event with $PM_{2.5}$ concentrations at 154 μg/m^3 at the urban site and 151 μg/m^3 at the mountain site, SO_4^{2-}/EC, NO_3^-/EC, and $PM_{2.5}$/EC factors dramatically increased (Figures 5a-b). Figures 5a-b show that SO_4^{2-}/EC and NO_3^-/EC factors reached their maximum values at the two sampling sites during the heavy Haze-I event, suggesting that massive secondary sulfates and nitrates formed during Haze-I evolution. In contrast, SO_4^{2-}/EC and NO_3^-/EC factors began to decrease, but OC/EC, K^+/EC, and $PM_{2.5}$/EC factors significantly increased during the Haze-II event, although $PM_{2.5}$ concentrations became even further elevated to 223 μg/m^3 at the urban site and 185 μg/m^3 at the mountain site (Figures 5a-b). This result indicates that large amounts of aerosol including OM and K^+ contributed to the conversion from the Haze-I to the Haze-II events.

Individual particle analysis shows consistent results with the variation of X/EC factors described above: the fractions of OM, S-OM, and soot-containing particles only had minor changes at 6-9% (i.e., 9% to 18%, 23% to 29%, and 14% to 23%) at the urban site and at 2-3% (i.e., 9% to 11%, 61% to 64%, and 21% to 18%) at the mountain site from the clean day to the moderate Haze-I event (Figure 4). However, along with the moderate Haze-I evolving into the heavy Haze-I event, S-OM fractions suddenly increased from 29% to 60% at the urban site and from 64% to 74% at the

https://doi.org/10.5194/acp-2019-1025
Preprint. Discussion started: 8 January 2020
© Author(s) 2020. CC BY 4.0 License.

Atmospheric Chemistry and Physics Discussions

mountain site (Figure 4). When the heavy Haze-I turned into the Haze-II events, S-OM fractions significantly decreased from 60-74% to 30-32% at two sampling sites but K-OM fractions largely increased from 4-5% to 50-52% (Figure 4). As a result, the chemical data of $PM_{2.5}$ samples and individual particle analysis both well reflect the haze evolution and transformation.

4. Discussion

4.1 Sources and formation of two distinctive haze events

Our analyses show that the fractions of OM in $PM_{2.5}$ by mass (35-41%, Figures 2a-c) and OM-containing in individual particles by number (> 70%, Figure 4) both were elevated during the Haze-I event at the urban and mountain sites. TEM observations showed two major types of OM particles: spherical OM and domelike OM during the Haze-I event (Figures 6c-d). These OM particles have been considered as primary OM aerosol, which can indicate the direct emissions from residential coal burning (Zhang et al., 2018a) or biomass burning (Liu et al., 2017a). In addition, we noticed that K-OM particles as a tracer of biomass burning (Adachi and Buseck, 2008; Bi et al., 2011; Liu et al., 2017a) were quite low at ~3% by number fraction during the Haze-I event (Figure 4) and had poor correlations with $PM_{2.5}$ concentrations (Figure 7a). Therefore, we can exclude biomass burning and conclude that coal burning was the major contribution to emissions during the Haze-I event. During the wintertime with the lowest temperature at about -30 °C in Northeast China, high-intensity coal burning activities for household heating are necessary (Xu et al., 2017; Zhang et al., 2017). Central heating through large boilers equipped with efficient filters are in wide use in the urban areas in Northeast China, but residential stoves without emission controls are still used for household heating and cooking in the rural and suburban areas (Zhang et al., 2017). Through the meteorological data (Figures S3a-b) and air mass backward trajectory (Figure 7c) analyses, we inferred that the air at the two sampling sites during the Haze-I event was mostly influenced by Shenyang city and its

https://doi.org/10.5194/acp-2019-1025
Preprint. Discussion started: 8 January 2020
© Author(s) 2020. CC BY 4.0 License.

Atmospheric Chemistry and Physics Discussions

nearby surrounding emissions. As a result, we determined that large amounts of fine primary OM aerosol during the Haze-I event were mainly from regional emissions of coal burning in residential stoves for heating and cooking as shown in Figure 8.

The significant increases of SO_4^{2-}/EC, NO_3^-/EC, and $PM_{2.5}$/EC factors from the moderate to heavy Haze-I event (Figures 5a-b) suggest that massive secondary production of sulfates and nitrates elevated $PM_{2.5}$ concentrations. Similar results that secondary aerosol formation causes heavy winter hazes in the NCP have been well documented (Liu et al., 2017c; Sun et al., 2014; Xue et al., 2016; Zheng et al., 2015a). Although photochemical activity is weak because of thick haze layers weakening solar radiation (Zhao et al., 2013; Zheng et al., 2015b), heterogeneous chemical reactions on particle surfaces have been considered as major pathways in the formation of sulfates and nitrates from SO_2 and NO_x whenever RH exceeds 70% (Sun et al., 2018; Wang et al., 2016; Wu et al., 2018). Here, TEM observations did show that large numbers of primary OM particles were coated by S-rich aerosols at 73-80% of RH during the heavy Haze-I event (Figures 6c-d). Obviously, the preexisting particles in the hazes provided large heterogeneous surfaces for the formation of sulfates and nitrates (He et al., 2014; Li et al., 2011; Zhang et al., 2017). When the moderate Haze-I turned into the heavy Haze-I event, we indeed found that secondary inorganic ions (i.e., SO_4^{2-}, NO_3^-, and NH_4^+) became the predominant species in $PM_{2.5}$, accounting for 62-66% (Figures 2a-c). Therefore, we conclude that atmospheric heterogeneous reactions under high RH (> 70%) are a critical factor in heavy haze formation in Northeast China.

In contrast to the Haze-I event, we found that concentrations of K^+ and OM in $PM_{2.5}$ both were elevated about twice as much during the Haze-II event (Figures 2b-c). In addition, TEM observations showed that the fraction of K-OM particles explosively increased by 45-48% during the Haze-II event (Figure 4). High levels of K^+ or K-OM particles represent the influences of biomass burning (Bi et al., 2011; Liu et al., 2017a). Indeed, MODIS data during the Haze-II event show that many fire

https://doi.org/10.5194/acp-2019-1025
Preprint. Discussion started: 8 January 2020
© Author(s) 2020. CC BY 4.0 License.

Atmospheric Chemistry and Physics Discussions

436 spots occurred in the north part of Northeast China, far away ~580 km from sampling
437 sites, and the air mass backward trajectories at the urban and mountain sites both
438 crossed these fire spots (Figure 7d). MODIS maps further show that these fire spots
439 were in the farming lands instead of the forest areas (Figure 7d). Based on the MODIS
440 data and reports from the local department of ecology and environment
441 (http://www.hljdep.gov.cn/hjgl/zfjc/jphz/2017/05/15698.html), these dense fire spots
442 on 4 November were agricultural biomass burning. Open agricultural biomass burning
443 is normally intense during the early winter in Northeast China, a region with abundant
444 agricultural production, because large amounts of agricultural waste need to be
445 cleaned up and their burnt products can be used as fertilizers to increase soil fertility
446 (Cao et al., 2017; Yang et al., 2017). Along with the backward trajectories of air
447 masses, we found sharp $PM_{2.5}$ concentrations occurring from Harbin city (1281 μg/m^3
448 at 18:00 on 4 November) to Changchun city (658 μg/m^3 at 0:00 on 5 November) and
449 to Shenyang city (669 μg/m^3 at 8:00 on 5 November) (Figure S5a). These above
450 analyses well indicated that long-range transport of agricultural biomass burning
451 emissions directly led to the Haze-II formation (Figure 8) and explained why K^+/EC,
452 OC/EC, and $PM_{2.5}$/EC factors together reached their maximum values during the
453 Haze-II event (Figures 5a-b) and K-OM fractions and $PM_{2.5}$ mass concentrations had
454 strong positive correlation (Figure 7b). Overall, although the Haze-II and Haze-I
455 events both displayed heavy pollution levels, they had contrasting emission sources
456 and formation mechanisms as illustrated in Figure 8.
457
458 **4.2 Comparison: haze in Northeast China vs. NCP**
459 OC/EC ratios in $PM_{2.5}$ of 8.0-10.6 during the Haze-I event and 25.4-27.9 during
460 the Haze-II event were reported in Northeast China in this study (Table S1). The
461 results are much higher than OC/EC ratios in $PM_{2.5}$ during winter haze episodes in the
462 NCP, such as 4.5 in Beijing city (Zhao et al., 2013), 5.5 in Jinan city (Chen et al.,
463 2017b), and 5.3 in Tianjin city (Han et al., 2014). In addition, TEM observations

https://doi.org/10.5194/acp-2019-1025
Preprint. Discussion started: 8 January 2020
© Author(s) 2020. CC BY 4.0 License.

Atmospheric Chemistry and Physics Discussions

showed that OM-containing particles were dominant by number fraction (e.g., 75-96% during the Haze-I event and 96-97% during the Haze-II event) in Northeast China (Figure 4). The results are higher than 50-70% during regional haze episodes in the NCP which were influenced by residential coal burning (Chen et al., 2017b; Li et al., 2012). These comparisons suggest that the contribution of residential coal burning and biomass burning to winter haze formation in Northeast China is significantly larger than that in the NCP. Moreover, fly ash/metal-containing particles as the tracers of industry emissions frequently occurred in regional hazes in the NCP, such as ~30% by number fraction in Jinan city (Li et al., 2011), 23-29% in Beijing city (Ma et al., 2016), and 13-17% in Xianghe (Zou et al., 2019). These data are much higher than 8% (Haze-I) and 1% (Haze-II) reported in this study (Figure 4), suggesting that the contribution of industrial emissions to regional haze in Northeast China is much smaller than that in the NCP. Many studies have summarized formation mechanisms of general regional haze in North China: regional transport of air pollutants (Zheng et al., 2015b), massive formation of secondary aerosols (Shao et al., 2019), and two-way feedback between adverse meteorological conditions and pollutant accumulation (Zhong et al., 2019). We found that the Haze-I formation in this study can be attributed to these three formation mechanisms (Figure 8). Moreover, the Haze-II formation indicates that the primary emissions from intensive agricultural biomass burning activities can rapidly induce regional heavy haze formation in Northeast China (Figure 8).

5. Atmospheric implications

High concentrations of $PM_{2.5}$ in haze adversely affect human health by inducing various respiratory diseases (Cohen et al., 2017; Liu et al., 2016). In China, long-term exposure to high levels of ambient $PM_{2.5}$ has resulted in 1.1-1.35 million premature deaths (Cohen et al., 2017; Lelieveld et al., 2015). The large-scale coal burning for household heating and cooking in Northeast China emits vast numbers of

https://doi.org/10.5194/acp-2019-1025
Preprint. Discussion started: 8 January 2020
© Author(s) 2020. CC BY 4.0 License.

Atmospheric Chemistry and Physics Discussions

492 OM-containing particles (discussed in Section 4.1), which include abundant
493 polycyclic aromatic hydrocarbons (PAHs) (Chen et al., 2017b; Chen et al., 2013;
494 Zhang et al., 2008). Based on Ebenstein et al. (2017), people's life expectancy
495 decreases by 0.64 years for every 10 μg/m^3 contributed by residential coal burning
496 emissions. Furthermore, we found that 1-8% of haze particles contained toxic metals
497 (e.g., Pb, Zn, Cr, and Mn) from fly ash/metal particles with sizes smaller than 100 nm
498 in Northeast China (Figures 4 and S6a-b). Oberdorster et al. (2004) indicated that
499 such ultrafine metal particles can exert adverse health impacts via deposition in
500 human lungs and further penetration into the blood. Therefore, these OM-containing
501 and fly ash/metal-containing particles observed by TEM (Figures 6a-f) are harmful to
502 human health in Northeast China in winter.

503 The light-absorbing particles (i.e., BC and BrC) have been proved to reduce solar
504 radiation reaching the ground and further influence regional climate and crop
505 production (Alexander et al., 2008; Bond et al., 2013; Tie et al., 2016; Wang et al.,
506 2018). This study shows that concentrations of BC (i.e., EC or soot) were low at
507 2.7-4.3 μg/m^3 during the haze days and only accounted for 1.4-3.9% of $PM_{2.5}$ in
508 Northeast China (Figures 2a-c). These results are lower than them in other regions of
509 China such as the NCP: 7.6 μg/m^3 and 5.2% in Beijing city (Wu et al., 2016), Yangtze
510 River Delta: 11.8 μg/m^3 and 4.4% in Shanghai city (Zhi et al., 2014), and Pearl River
511 Delta: 9.6 μg/m^3 and 7.7% in Guangzhou city (Tao et al., 2012). These comparisons
512 indicate that BC concentrations are at low levels in Northeast China during winter
513 haze periods, although $PM_{2.5}$ concentrations are extremely high. Furthermore, TEM
514 observations showed that 75-97% of haze particles were OM-containing particles
515 such as spherical OM and domelike OM, but only 4-23% were soot-containing
516 particles in Northeast China (Figure 4). Previous studies have demonstrated that these
517 spherical and domelike OM particles from coal and biomass burning with low
518 combustion efficiency are tarballs (Chakrabarty et al., 2010; Hand et al., 2005; Pósfai
519 et al., 2004; Zhang et al., 2018a) or precursors of tarballs (Adachi et al., 2019;

https://doi.org/10.5194/acp-2019-1025
Preprint. Discussion started: 8 January 2020
© Author(s) 2020. CC BY 4.0 License.

Atmospheric Chemistry and Physics Discussions

Sedlacek III et al., 2018; Tóth et al., 2014), respectively. Tarballs as the primary BrC have a wide absorption spectrum from visible to ultraviolet wavelengths (Hoffer et al., 2016). The comparison in Section 4.2 indicates that the highest emission of tarballs in China during winter occurs in Northeast China because of the intense and inefficient residential coal burning and agricultural biomass burning. Therefore, how large numbers of tarballs in regional winter haze influence atmospheric optical radiation and climate in Northeast China should be studied in much greater detail.

Implementing suitable policies to encourage cleaner energy use (e.g., natural gas and electricity) instead of coal and biomass for household heating are necessary in Northeast China. Such policies would not only reduce regional haze formation but also reduce the toxic aerosol components in the air. Admittedly, this transition of heating energy would be facing a monumental challenge in Northeast China due to its low economic growth and its low urbanization development rates (Zhao et al., 2018a). Moreover, how to control open agricultural biomass burning should be considered in Northeast China. Over the past decades, agricultural biomass returned to soils and recycling agricultural biomass have both failed in Northeast China. This failure arises because agricultural biomass does not decay throughout the winter with its low temperatures down to -30 °C and snow or ice covers and its recycling consumes a lot of manpower, material resources, and money (Yan et al., 2006). Therefore, how to deal with agricultural biomass waste in Northeast China should be carefully thought out by the local farmers in concert with the government.

6. Conclusions

To understand the formation mechanisms of winter haze in Northeast China, we carried out an aerosol experiment at an urban site and a mountain site in the south part of Northeast China from 31 October to 6 November 2016. Two different regional heavy haze events (Haze-I and Haze-II) were identified during the sampling period. Chemical composition (water-soluble ions, OM, and EC) of $PM_{2.5}$ were obtained using

https://doi.org/10.5194/acp-2019-1025
Preprint. Discussion started: 8 January 2020
© Author(s) 2020. CC BY 4.0 License.

Atmospheric Chemistry and Physics Discussions

548 ion chromatography and OC/EC analysis. Types and mixing states of individual
549 particles were identified using TEM/EDS and NanoSIMS: mineral, fly
550 ash/metal-containing, soot-containing, OM, S-OM, K-OM, and OM-containing.
551 Haze-I event has an evolution process from moderate to heavy pollution. OM was
552 the dominant component in $PM_{2.5}$ and their concentrations were 45 μg/m^3 at the urban
553 site and 39 μg/m^3 at the mountain site during the moderate Haze-I event. Individual
554 particle analysis also showed that over 70% of particles contained OM during the
555 moderate Haze-I event. Following the Haze-I evolution, secondary inorganic ions (i.e.,
556 SO_4^{2-}, NO_3^-, and NH_4^+) became the dominant components (94-101 μg/m^3) during the
557 heavy Haze-I event with $PM_{2.5}$ concentrations of 151-154 μg/m^3. Similarly, the number
558 fractions of S-OM increased from 29% to 60% at the urban site and from 64% to 74%
559 at the mountain site from the moderate Haze-I to the heavy Haze-I event. Along with
560 the prevailing wind suddenly changing from southerly with ~0.8 m/s to northerly with
561 ~3.9 m/s, the heavy Haze-I rapidly turned into the Haze-II events with $PM_{2.5}$
562 concentrations of 185-223 μg/m^3. Meanwhile, OM replaced secondary inorganic ions
563 as the dominant component in $PM_{2.5}$ during the Haze-II event, accounting for 53-60%.
564 Furthermore, K^+ concentration during the Haze-II event was about three times higher
565 than that during the heavy Haze-I event. Individual particle analysis showed
566 consistent results that the number fractions of K-OM significantly increased from 4-5%
567 to 50-52%.
568 Based on our study, the accumulation of primary OM particles, mainly emitted
569 from residential coal burning, induced the moderate Haze-I formation with the onset of
570 stable meteorological conditions. Production of secondary aerosols via heterogeneous
571 reactions at high RH (> 70%), in particular sulfates and nitrates, caused the transition
572 from the moderate Haze-I to the heavy Haze-I. Furthermore, the long-range transport
573 of primary emissions from intense agricultural biomass burning led to the Haze-II
574 formation in the downwind areas in Northeast China. Our study also reveals that the
575 significant light-absorbing particles in Northeast China during winter are tarballs,

https://doi.org/10.5194/acp-2019-1025
Preprint. Discussion started: 8 January 2020
© Author(s) 2020. CC BY 4.0 License.

Atmospheric Chemistry and Physics Discussions

576 which is different from other regions in China influenced by serious air pollution.

https://doi.org/10.5194/acp-2019-1025
Preprint. Discussion started: 8 January 2020
© Author(s) 2020. CC BY 4.0 License.

Atmospheric Chemistry and Physics Discussions

577 **Author contributions**

578 JZ and WL conceived the study and wrote the manuscript. The field campaign was
579 organized and supervised by JZ and WL, and assisted by LL, LX, and HZ. JZ, LL, LX,
580 and QL contributed the sample analyses. All authors reviewed and commented on the
581 paper.

582

583 **Acknowledgements**

584 We appreciate Peter Hyde's comments and proofreading. We thank Jiaxing Sun
585 and Yong Ren for their assistance of sample collections. This work was funded by the
586 National Key R&D Program of China (2017YFC0212700), National Natural Science
587 Foundation of China (91844301, 41622504, 41575116), Zhejiang Provincial Natural
588 Science Foundation of China (LZ19D050001), and Zhejiang University Education
589 Foundation Global Partnership Fund (188170-11103/004). All data presented in this
590 paper are available upon request from the corresponding author (W. J. Li, e-mail:
591 liweijun@zju.edu.cn).

https://doi.org/10.5194/acp-2019-1025
Preprint. Discussion started: 8 January 2020
© Author(s) 2020. CC BY 4.0 License.

Atmospheric Chemistry and Physics Discussions

References

Adachi, K., and Buseck, P. R.: Internally mixed soot, sulfates, and organic matter in aerosol particles from Mexico City, Atmos. Chem. Phys., 8, 6469-6481, https://doi.org/10.5194/acp-8-6469-2008, 2008.

Adachi, K., Sedlacek, A. J., Kleinman, L., Springston, S. R., Wang, J., Chand, D., Hubbe, J. M., Shilling, J. E., Onasch, T. B., Kinase, T., Sakata, K., Takahashi, Y., and Buseck, P. R.: Spherical tarball particles form through rapid chemical and physical changes of organic matter in biomass-burning smoke, P. Natl. Acad. Sci. USA, 116, 19336-19341, https://doi.org/10.1073/pnas.1900129116, 2019.

Alexander, D. T. L., Crozier, P. A., and Anderson, J. R.: Brown carbon spheres in East Asian outflow and their optical properties, Science, 321, 833-836, https://doi.org/10.1126/science.1155296, 2008.

Bennartz, R., Fan, J., Rausch, J., Leung, L. R., and Heidinger, A. K.: Pollution from China increases cloud droplet number, suppresses rain over the East China Sea, Geophys. Res. Lett., 38, L09704, https://doi.org/10.1029/2011GL047235, 2011.

Bi, X., Zhang, G., Li, L., Wang, X., Li, M., Sheng, G., Fu, J., and Zhou, Z.: Mixing state of biomass burning particles by single particle aerosol mass spectrometer in the urban area of PRD, China, Atmos. Environ., 45, 3447-3453, https://doi.org/10.1016/j.atmosenv.2011.03.034, 2011.

Bond, T. C., Doherty, S. J., Fahey, D. W., Forster, P. M., Berntsen, T., DeAngelo, B. J., Flanner, M. G., Ghan, S., Kärcher, B., Koch, D., Kinne, S., Kondo, Y., Quinn, P. K., Sarofim, M. C., Schultz, M. G., Schulz, M., Venkataraman, C., Zhang, H., Zhang, S., Bellouin, N., Guttikunda, S. K., Hopke, P. K., Jacobson, M. Z., Kaiser, J. W., Klimont, Z., Lohmann, U., Schwarz, J. P., Shindell, D., Storelvmo, T., Warren, S. G., and Zender, C. S.: Bounding the role of black carbon in the climate system: A scientific assessment, J. Geophys. Res.-Atmos., 118, 5380-5552, https://doi.org/10.1002/jgrd.50171, 2013.

Cao, F., Zhang, S. C., Kawamura, K., Liu, X., Yang, C., Xu, Z., Fan, M., Zhang, W., Bao, M., Chang, Y., Song, W., Liu, S., Lee, X., Li, J., Zhang, G., and Zhang, Y. L.: Chemical characteristics of dicarboxylic acids and related organic compounds in PM2.5 during biomass-burning and non-biomass-burning seasons at a rural site of Northeast China, Environ. Pollut., 231, 654-662, https://doi.org/10.1016/j.envpol.2017.08.045, 2017.

Chakrabarty, R. K., Moosmüller, H., Chen, L. W. A., Lewis, K., Arnott, W. P., Mazzoleni, C., Dubey, M. K., Wold, C. E., Hao, W. M., and Kreidenweis, S. M.: Brown carbon in tar balls from smoldering biomass combustion, Atmos. Chem. Phys., 10, 6363-6370, https://doi.org/10.5194/acp-10-6363-2010, 2010.

Chen, C., Li, H., Niu, Y., Liu, C., Lin, Z., Cai, J., Li, W., Ge, W., Chen, R., and Kan, H.: Impact of short-term exposure to fine particulate matter air pollution on urinary metabolome: A randomized, double-blind, crossover trial, Environ. Int., 130, 104878, https://doi.org/10.1016/j.envint.2019.05.072, 2019.

Chen, J., Li, C., Ristovski, Z., Milic, A., Gu, Y., Islam, M. S., Wang, S., Hao, J., Zhang, H., He, C., Guo, H., Fu, H., Miljevic, B., Morawska, L., Thai, P., Lam, Y. F., Pereira, G., Ding, A., Huang, X., and Dumka, U. C.: A review of biomass burning: Emissions and impacts on air quality, health and climate in China, Sci. Total Environ., 579, 1000-1034,

https://doi.org/10.5194/acp-2019-1025
Preprint. Discussion started: 8 January 2020
© Author(s) 2020. CC BY 4.0 License.

https://doi.org/10.1016/j.scitotenv.2016.11.025, 2017a.

Chen, S., Xu, L., Zhang, Y., Chen, B., Wang, X., Zhang, X., Zheng, M., Chen, J., Wang, W., Sun, Y., Fu, P., Wang, Z., and Li, W.: Direct observations of organic aerosols in common wintertime hazes in North China: insights into direct emissions from Chinese residential stoves, Atmos. Chem. Phys., 17, 1259-1270, https://doi.org/10.5194/acp-17-1259-2017, 2017b.

Chen, W., Tong, D., Zhang, S., Dan, M., Zhang, X., and Zhao, H.: Temporal variability of atmospheric particulate matter and chemical composition during a growing season at an agricultural site in northeastern China, J. Environ. Sci., 38, 133-141, https://doi.org/10.1016/j.jes.2015.05.023, 2015.

Chen, Y., Ebenstein, A., Greenstone, M., and Li, H.: Evidence on the impact of sustained exposure to air pollution on life expectancy from China's Huai River policy, P. Natl. Acad. Sci. USA, 110, 12936-12941, https://doi.org/10.1073/pnas.1300018110, 2013.

Cheng, Y., Zheng, G., Wei, C., Mu, Q., Zheng, B., Wang, Z., Gao, M., Zhang, Q., He, K., Carmichael, G., Poschl, U., and Su, H.: Reactive nitrogen chemistry in aerosol water as a source of sulfate during haze events in China, Sci. Adv., 2, e1601530, https://doi.org/10.1126/sciadv.1601530, 2016.

Chi, J. W., Li, W. J., Zhang, D. Z., Zhang, J. C., Lin, Y. T., Shen, X. J., Sun, J. Y., Chen, J. M., Zhang, X. Y., Zhang, Y. M., and Wang, W. X.: Sea salt aerosols as a reactive surface for inorganic and organic acidic gases in the Arctic troposphere, Atmos. Chem. Phys., 15, 11341-11353, https://doi.org/doi:10.5194/acp-15-11341-2015, 2015.

Chowdhury, S., Dey, S., Guttikunda, S., Pillarisetti, A., Smith, K. R., and Di Girolamo, L.: Indian annual ambient air quality standard is achievable by completely mitigating emissions from household sources, P. Natl. Acad. Sci. USA, 116, 10711-10716, https://doi.org/10.1073/pnas.1900888116, 2019.

Cohen, A. J., Brauer, M., Burnett, R., Anderson, H. R., Frostad, J., Estep, K., Balakrishnan, K., Brunekreef, B., Dandona, L., Dandona, R., Feigin, V., Freedman, G., Hubbell, B., Jobling, A., Kan, H., Knibbs, L., Liu, Y., Martin, R., Morawska, L., Pope, C. A., Shin, H., Straif, K., Shaddick, G., Thomas, M., van Dingenen, R., van Donkelaar, A., Vos, T., Murray, C. J. L., and Forouzanfar, M. H.: Estimates and 25-year trends of the global burden of disease attributable to ambient air pollution: an analysis of data from the Global Burden of Diseases Study 2015, Lancet, 389, 1907-1918, https://doi.org/10.1016/s0140-6736(17)30505-6, 2017.

Ding, A. J., Huang, X., Nie, W., Sun, J. N., Kerminen, V. M., Petäjä, T., Su, H., Cheng, Y. F., Yang, X. Q., Wang, M. H., Chi, X. G., Wang, J. P., Virkkula, A., Guo, W. D., Yuan, J., Wang, S. Y., Zhang, R. J., Wu, Y. F., Song, Y., Zhu, T., Zilitinkevich, S., Kulmala, M., and Fu, C. B.: Enhanced haze pollution by black carbon in megacities in China, Geophys. Res. Lett., 43, 2873-2879, https://doi.org/10.1002/2016GL067745, 2016.

Ebenstein, A., Fan, M., Greenstone, M., He, G., and Zhou, M.: New evidence on the impact of sustained exposure to air pollution on life expectancy from China's Huai River Policy, P. Natl. Acad. Sci. USA, 114, 10384-10389, https://doi.org/10.1073/pnas.1616784114, 2017.

Fortems‐Cheiney, A., Dufour, G., Hamaoui‐Laguel, L., Foret, G., Siour, G., Van Damme, M., Meleux, F., Coheur, P. F., Clerbaux, C., and Clarisse, L.: Unaccounted variability in NH_3 agricultural sources detected by IASI contributing to European spring haze episode, Geophys. Res.

https://doi.org/10.5194/acp-2019-1025
Preprint. Discussion started: 8 January 2020
© Author(s) 2020. CC BY 4.0 License.

Lett., 43, 5475-5482, https://doi.org/10.1002/2016GL069361, 2016.

Frossard, A. A., Shaw, P. M., Russell, L. M., Kroll, J. H., Canagaratna, M. R., Worsnop, D. R., Quinn, P. K., and Bates, T. S.: Springtime Arctic haze contributions of submicron organic particles from European and Asian combustion sources, J. Geophys. Res., 116, D05205, https://doi.org/10.1029/2010JD015178, 2011.

Gao, J., Woodward, A., Vardoulakis, S., Kovats, S., Wilkinson, P., Li, L., Xu, L., Li, J., Yang, J., Li, J., Cao, L., Liu, X., Wu, H., and Liu, Q.: Haze, public health and mitigation measures in China: A review of the current evidence for further policy response, Sci. Total Environ., 578, 148-157, https://doi.org/10.1016/j.scitotenv.2016.10.231, 2017.

Guinot, B., Cachier, H., and Oikonomou, K.: Geochemical perspectives from a new aerosol chemical mass closure, Atmos. Chem. Phys., 7, 1657-1670, https://doi.org/10.5194/acp-7-1657-2007, 2007.

Guo, S., Hu, M., Zamora, M. L., Peng, J., Shang, D., Zheng, J., Du, Z., Wu, Z., Shao, M., Zeng, L., Molina, M. J., and Zhang, R.: Elucidating severe urban haze formation in China, P. Natl. Acad. Sci. USA, 111, 17373-17378, https://doi.org/10.1073/pnas.1419604111, 2014.

Han, S., Wu, J., Zhang, Y., Cai, Z., Feng, Y., Yao, Q., Li, X., Liu, Y., and Zhang, M.: Characteristics and formation mechanism of a winter haze–fog episode in Tianjin, China, Atmos. Environ., 98, 323-330, https://doi.org/10.1016/j.atmosenv.2014.08.078, 2014.

Hand, J. L., Malm, W. C., Laskin, A., Day, D., Lee, T., Wang, C., Carrico, C., Carrillo, J., Cowin, J. P., Collett, J., and Iedema, M. J.: Optical, physical, and chemical properties of tar balls observed during the Yosemite Aerosol Characterization Study, J. Geophys. Res., 110, D21210, https://doi.org/10.1029/2004JD005728, 2005.

He, H., Wang, Y., Ma, Q., Ma, J., Chu, B., Ji, D., Tang, G., Liu, C., Zhang, H., and Hao, J.: Mineral dust and NOx promote the conversion of SO_2 to sulfate in heavy pollution days, Sci. Rep., 4, 4172, https://doi.org/10.1038/srep04172, 2014.

Hoffer, A., Tóth, A., Nyirő-Kósa, I., Pósfai, M., and Gelencsér, A.: Light absorption properties of laboratory-generated tar ball particles, Atmos. Chem. Phys., 16, 239-246, https://doi.org/10.5194/acp-16-239-2016, 2016.

Huang, R. J., Zhang, Y., Bozzetti, C., Ho, K. F., Cao, J. J., Han, Y., Daellenbach, K. R., Slowik, J. G., Platt, S. M., Canonaco, F., Zotter, P., Wolf, R., Pieber, S. M., Bruns, E. A., Crippa, M., Ciarelli, G., Piazzalunga, A., Schwikowski, M., Abbaszade, G., Schnelle-Kreis, J., Zimmermann, R., An, Z., Szidat, S., Baltensperger, U., El Haddad, I., and Prevot, A. S.: High secondary aerosol contribution to particulate pollution during haze events in China, Nature, 514, 218-222, https://doi.org/10.1038/nature13774, 2014.

Huang, Y., Li, L., Li, J., Wang, X., Chen, H., Chen, J., Yang, X., Gross, D. S., Wang, H., Qiao, L., and Chen, C.: A case study of the highly time-resolved evolution of aerosol chemical and optical properties in urban Shanghai, China, Atmos. Chem. Phys., 13, 3931-3944, https://doi.org/10.5194/acp-13-3931-2013, 2013.

Jung, J., Lee, K., Cayetano, M. G., Batmunkh, T., and Kim, Y. J.: Optical and hygroscopic properties of long-range transported haze plumes observed at Deokjeok Island off the west coast of the Korean Peninsula under the Asian continental outflows, J. Geophys. Res.-Atmos., 120, 8861-8877, https://doi.org/10.1002/2015JD023154, 2015.

https://doi.org/10.5194/acp-2019-1025
Preprint. Discussion started: 8 January 2020
© Author(s) 2020. CC BY 4.0 License.

Atmospheric Chemistry and Physics Discussions

718 Lelieveld, J., Evans, J. S., Fnais, M., Giannadaki, D., and Pozzer, A.: The contribution of outdoor
719 air pollution sources to premature mortality on a global scale, Nature, 525, 367-371,
720 https://doi.org/10.1038/nature15371, 2015.
721 Li, M., Wang, T., Xie, M., Li, S., Zhuang, B., Huang, X., Chen, P., Zhao, M., and Liu, J.:
722 Formation and Evolution Mechanisms for Two Extreme Haze Episodes in the Yangtze River Delta
723 Region of China During Winter 2016, J. Geophys. Res.-Atmos., 124, 3607-3623,
724 https://doi.org/10.1029/2019JD030535, 2019.
725 Li, P., Yan, R., Yu, S., Wang, S., Liu, W., and Bao, H.: Reinstate regional transport of $PM_{2.5}$ as a
726 major cause of severe haze in Beijing, P. Natl. Acad. Sci. USA, 112, E2739-E2740,
727 https://doi.org/10.1073/pnas.1502596112, 2015.
728 Li, W., and Shao, L.: Transmission electron microscopy study of aerosol particles from the brown
729 hazes in northern China, J. Geophys. Res., 114, D09302, https://doi.org/10.1029/2008JD011285,
730 2009.
731 Li, W., Zhou, S., Wang, X., Xu, Z., Yuan, C., Yu, Y., Zhang, Q., and Wang, W.: Integrated
732 evaluation of aerosols from regional brown hazes over northern China in winter: Concentrations,
733 sources, transformation, and mixing states, J. Geophys. Res., 116, D09301,
734 https://doi.org/10.1029/2010JD015099, 2011.
735 Li, W., Shi, Z., Zhang, D., Zhang, X., Li, P., Feng, Q., Yuan, Q., and Wang, W.: Haze particles
736 over a coal-burning region in the China Loess Plateau in winter: Three flight missions in
737 December 2010, J. Geophys. Res., 117, D12306, https://doi.org/10.1029/2012JD017720, 2012.
738 Li, W., Sun, J., Xu, L., Shi, Z., Riemer, N., Sun, Y., Fu, P., Zhang, J., Lin, Y., Wang, X., Shao, L.,
739 Chen, J., Zhang, X., Wang, Z., and Wang, W.: A conceptual framework for mixing structures in
740 individual aerosol particles, J. Geophys. Res.-Atmos., 121, 13784-13798,
741 https://doi.org/10.1002/2016JD025252, 2016.
742 Li, W., Xu, L., Liu, X., Zhang, J., Lin, Y., Yao, X., Gao, H., Zhang, D., Chen, J., and Wang, W.:
743 Air pollution–aerosol interactions produce more bioavailable iron for ocean ecosystems, Sci. Adv.,
744 3, e1601749, https://doi.org/10.1126/sciadv.1601749, 2017a.
745 Li, X., Ma, Y., Wang, Y., Liu, N., and Hong, Y.: Temporal and spatial analyses of particulate
746 matter (PM_{10} and $PM_{2.5}$) and its relationship with meteorological parameters over an urban city in
747 northeast China, Atmos. Res., 198, 185-193, https://doi.org/10.1016/j.atmosres.2017.08.023,
748 2017b.
749 Li, Z., Guo, J., Ding, A., Liao, H., Liu, J., Sun, Y., Wang, T., Xue, H., Zhang, H., and Zhu, B.:
750 Aerosol and boundary-layer interactions and impact on air quality, Natl. Sci. Rev., 4, 810-833,
751 https://doi.org/10.1093/nsr/nwx117, 2017c.
752 Lin, M., Biglari, S., Zhang, Z., Crocker, D., Tao, J., Su, B., Liu, L., and Thiemens, M. H.:
753 Vertically uniform formation pathways of tropospheric sulfate aerosols in East China detected
754 from triple stable oxygen and radiogenic sulfur isotopes, Geophys. Res. Lett., 44, 5187-5196,
755 https://doi.org/10.1002/2017GL073637, 2017.
756 Liu, D., Joshi, R., Wang, J., Yu, C., Allan, J. D., Coe, H., Flynn, M. J., Xie, C., Lee, J., Squires, F.,
757 Kotthaus, S., Grimmond, S., Ge, X., Sun, Y., and Fu, P.: Contrasting physical properties of black
758 carbon in urban Beijing between winter and summer, Atmos. Chem. Phys., 19, 6749-6769,
759 https://doi.org/10.5194/acp-19-6749-2019, 2019.

https://doi.org/10.5194/acp-2019-1025
Preprint. Discussion started: 8 January 2020
© Author(s) 2020. CC BY 4.0 License.

Atmospheric Chemistry and Physics Discussions

760 Liu, J., Han, Y., Tang, X., Zhu, J., and Zhu, T.: Estimating adult mortality attributable to $PM_{2.5}$
761 exposure in China with assimilated $PM_{2.5}$ concentrations based on a ground monitoring network,
762 Sci. Total Environ., 568, 1253-1262, https://doi.org/10.1016/j.scitotenv.2016.05.165, 2016.
763 Liu, L., Kong, S., Zhang, Y., Wang, Y., Xu, L., Yan, Q., Lingaswamy, A. P., Shi, Z., Lv, S., Niu, H.,
764 Shao, L., Hu, M., Zhang, D., Chen, J., Zhang, X., and Li, W.: Morphology, composition, and
765 mixing state of primary particles from combustion sources-crop residue, wood, and solid waste,
766 Sci. Rep., 7, 5047, https://doi.org/10.1038/s41598-017-05357-2, 2017a.
767 Liu, M., Song, Y., Zhou, T., Xu, Z., Yan, C., Zheng, M., Wu, Z., Hu, M., Wu, Y., and Zhu, T.: Fine
768 particle pH during severe haze episodes in northern China, Geophys. Res. Lett., 44, 5213-5221,
769 https://doi.org/10.1002/2017GL073210, 2017b.
770 Liu, Y., Wu, Z., Wang, Y., Xiao, Y., Gu, F., Zheng, J., Tan, T., Shang, D., Wu, Y., Zeng, L., Hu, M.,
771 Bateman, A. P., and Martin, S. T.: Submicrometer Particles Are in the Liquid State during Heavy
772 Haze Episodes in the Urban Atmosphere of Beijing, China, Environ. Sci. Technol. Lett., 4,
773 427-432, https://doi.org/10.1021/acs.estlett.7b00352, 2017c.
774 Ma, L., Li, M., Zhang, H., Li, L., Huang, Z., Gao, W., Chen, D., Fu, Z., Nian, H., Zou, L., Gao, J.,
775 Chai, F., and Zhou, Z.: Comparative analysis of chemical composition and sources of aerosol
776 particles in urban Beijing during clear, hazy, and dusty days using single particle aerosol mass
777 spectrometry, J. Clean. Prod., 112, 1319-1329, https://doi.org/10.1016/j.jclepro.2015.04.054, 2016.
778 Ma, Y., Zhao, H., Dong, Y., Che, H., Li, X., Hong, Y., Li, X., Yang, H., Liu, Y., Wang, Y., Liu, N.,
779 and Sun, C.: Comparison of Two Air Pollution Episodes over Northeast China in Winter 2016/17
780 Using Ground-Based Lidar, J. Meteorol. Res., 32, 313-323,
781 https://doi.org/10.1007/s13351-018-7047-4, 2018.
782 Mahowald, N. M., Hamilton, D. S., Mackey, K. R. M., Moore, J. K., Baker, A. R., Scanza, R. A.,
783 and Zhang, Y.: Aerosol trace metal leaching and impacts on marine microorganisms, Nat.
784 Commun., 9, 2614, https://doi.org/10.1038/s41467-018-04970-7, 2018.
785 Miao, Y., Guo, J., Liu, S., Zhao, C., Li, X., Zhang, G., Wei, W., and Ma, Y.: Impacts of synoptic
786 condition and planetary boundary layer structure on the trans-boundary aerosol transport from
787 Beijing-Tianjin-Hebei region to northeast China, Atmos. Environ., 181, 1-11,
788 https://doi.org/10.1016/j.atmosenv.2018.03.005, 2018.
789 Oberdorster, G., Sharp, Z., Atudorei, V., Elder, A., Gelein, R., Kreyling, W., and Cox, C.:
790 Translocation of inhaled ultrafine particles to the brain, Inhal. Toxicol., 16, 437-445,
791 https://doi.org/10.1080/08958370490439597, 2004.
792 Pósfai, M., Gelencsér, A., Simonics, R., Arató, K., Li, J., Hobbs, P. V., and Buseck, P. R.:
793 Atmospheric tar balls: Particles from biomass and biofuel burning, J. Geophys. Res., 109, D06213,
794 https://doi.org/10.1029/2003JD004169, 2004.
795 Ren, L., Fu, P., He, Y., Hou, J., Chen, J., Pavuluri, C. M., Sun, Y., and Wang, Z.: Molecular
796 distributions and compound-specific stable carbon isotopic compositions of lipids in wintertime
797 aerosols from Beijing, Sci. Rep., 6, 27481, https://doi.org/10.1038/srep27481, 2016.
798 Rodo, X., Curcoll, R., Robinson, M., Ballester, J., Burns, J. C., Cayan, D. R., Lipkin, W. I.,
799 Williams, B. L., Couto-Rodriguez, M., Nakamura, Y., Uehara, R., Tanimoto, H., and Morgui, J. A.:
800 Tropospheric winds from northeastern China carry the etiologic agent of Kawasaki disease from
801 its source to Japan, P. Natl. Acad. Sci. USA, 111, 7952-7957,

© Author(s) 2020. CC BY 4.0 License.

https://doi.org/10.1073/pnas.1400380111, 2014.

Sedlacek III, A. J., Buseck, P. R., Adachi, K., Onasch, T. B., Springston, S. R., and Kleinman, L.: Formation and evolution of tar balls from northwestern US wildfires, Atmos. Chem. Phys., 18, 11289-11301, https://doi.org/10.5194/acp-18-11289-2018, 2018.

Shao, J., Chen, Q., Wang, Y., Lu, X., He, P., Sun, Y., Shah, V., Martin, R. V., Philip, S., Song, S., Zhao, Y., Xie, Z., Zhang, L., and Alexander, B.: Heterogeneous sulfate aerosol formation mechanisms during wintertime Chinese haze events: air quality model assessment using observations of sulfate oxygen isotopes in Beijing, Atmos. Chem. Phys., 19, 6107-6123, https://doi.org/10.5194/acp-19-6107-2019, 2019.

Shi, G., Xu, J., Peng, X., Xiao, Z., Chen, K., Tian, Y., Guan, X., Feng, Y., Yu, H., Nenes, A., and Russell, A. G.: pH of Aerosols in a Polluted Atmosphere: Source Contributions to Highly Acidic Aerosol, Environ. Sci. Technol., 51, 4289-4296, https://doi.org/10.1021/acs.est.6b05736, 2017.

Shi, J., Wang, N., Gao, H., Baker, A. R., Yao, X., and Zhang, D.: Phosphorus solubility in aerosol particles related to particle sources and atmospheric acidification in Asian continental outflow, Atmos. Chem. Phys., 19, 847-860, https://doi.org/10.5194/acp-19-847-2019, 2019.

Sobhani, N., Kulkarni, S., and Carmichael, G. R.: Source sector and region contributions to black carbon and $PM_{2.5}$ in the Arctic, Atmos. Chem. Phys., 18, 18123-18148, https://doi.org/10.5194/acp-18-18123-2018, 2018.

Sun, J., Liu, L., Xu, L., Wang, Y., Wu, Z., Hu, M., Shi, Z., Li, Y., Zhang, X., Chen, J., and Li, W.: Key Role of Nitrate in Phase Transitions of Urban Particles: Implications of Important Reactive Surfaces for Secondary Aerosol Formation, J. Geophys. Res.-Atmos., 123, 1234-1243, https://doi.org/10.1002/2017JD027264, 2018.

Sun, Y., Jiang, Q., Wang, Z., Fu, P., Li, J., Yang, T., and Yin, Y.: Investigation of the sources and evolution processes of severe haze pollution in Beijing in January 2013, J. Geophys. Res.-Atmos., 119, 4380-4398, https://doi.org/10.1002/2014JD021641, 2014.

Tóth, A., Hoffer, A., Nyirő-Kósa, I., Pósfai, M., and Gelencsér, A.: Atmospheric tar balls: aged primary droplets from biomass burning?, Atmos. Chem. Phys., 14, 6669-6675, https://doi.org/10.5194/acp-14-6669-2014, 2014.

Tao, J., Cao, J.-J., Zhang, R.-J., Zhu, L., Zhang, T., Shi, S., and Chan, C.-Y.: Reconstructed light extinction coefficients using chemical compositions of $PM_{2.5}$ in winter in Urban Guangzhou, China, Adv. Atmos. Sci., 29, 359-368, https://doi.org/10.1007/s00376-011-1045-0, 2012.

Tao, M., Chen, L., Xiong, X., Zhang, M., Ma, P., Tao, J., and Wang, Z.: Formation process of the widespread extreme haze pollution over northern China in January 2013: Implications for regional air quality and climate, Atmos. Environ., 98, 417-425, https://doi.org/10.1016/j.atmosenv.2014.09.026, 2014.

Tian, H. Z., Zhu, C. Y., Gao, J. J., Cheng, K., Hao, J. M., Wang, K., Hua, S. B., Wang, Y., and Zhou, J. R.: Quantitative assessment of atmospheric emissions of toxic heavy metals from anthropogenic sources in China: historical trend, spatial distribution, uncertainties, and control policies, Atmos. Chem. Phys., 15, 10127-10147, https://doi.org/10.5194/acp-15-10127-2015, 2015.

Tie, X., Huang, R. J., Dai, W., Cao, J., Long, X., Su, X., Zhao, S., Wang, Q., and Li, G.: Effect of heavy haze and aerosol pollution on rice and wheat productions in China, Sci. Rep., 6, 29612,

https://doi.org/10.5194/acp-2019-1025
Preprint. Discussion started: 8 January 2020
© Author(s) 2020. CC BY 4.0 License.

https://doi.org/10.1038/srep29612, 2016.

van Donkelaar, A., Martin, R. V., Brauer, M., Hsu, N. C., Kahn, R. A., Levy, R. C., Lyapustin, A., Sayer, A. M., and Winker, D. M.: Global Estimates of Fine Particulate Matter using a Combined Geophysical-Statistical Method with Information from Satellites, Models, and Monitors, Environ. Sci. Technol., 50, 3762-3772, https://doi.org/10.1021/acs.est.5b05833, 2016.

Wang, G., Zhang, R., Gomez, M. E., Yang, L., Levy Zamora, M., Hu, M., Lin, Y., Peng, J., Guo, S., Meng, J., Li, J., Cheng, C., Hu, T., Ren, Y., Wang, Y., Gao, J., Cao, J., An, Z., Zhou, W., Li, G., Wang, J., Tian, P., Marrero-Ortiz, W., Secrest, J., Du, Z., Zheng, J., Shang, D., Zeng, L., Shao, M., Wang, W., Huang, Y., Wang, Y., Zhu, Y., Li, Y., Hu, J., Pan, B., Cai, L., Cheng, Y., Ji, Y., Zhang, F., Rosenfeld, D., Liss, P. S., Duce, R. A., Kolb, C. E., and Molina, M. J.: Persistent sulfate formation from London Fog to Chinese haze, P. Natl. Acad. Sci. USA, 113, 13630-13635, https://doi.org/10.1073/pnas.1616540113, 2016.

Wang, J., Nie, W., Cheng, Y., Shen, Y., Chi, X., Wang, J., Huang, X., Xie, Y., Sun, P., Xu, Z., Qi, X., Su, H., and Ding, A.: Light absorption of brown carbon in eastern China based on 3-year multi-wavelength aerosol optical property observations and an improved absorption Ångström exponent segregation method, Atmos. Chem. Phys., 18, 9061-9074, https://doi.org/10.5194/acp-18-9061-2018, 2018.

Wang, J., Liu, D., Ge, X., Wu, Y., Shen, F., Chen, M., Zhao, J., Xie, C., Wang, Q., Xu, W., Zhang, J., Hu, J., Allan, J., Joshi, R., Fu, P., Coe, H., and Sun, Y.: Characterization of black carbon-containing fine particles in Beijing during wintertime, Atmos. Chem. Phys., 19, 447-458, https://doi.org/10.5194/acp-19-447-2019, 2019.

Wang, Z., Li, J., Wang, Z., Yang, W., Tang, X., Ge, B., Yan, P., Zhu, L., Chen, X., Chen, H., Wand, W., Li, J., Liu, B., Wang, X., Wand, W., Zhao, Y., Lu, N., and Su, D.: Modeling study of regional severe hazes over mid-eastern China in January 2013 and its implications on pollution prevention and control, Sci. China Earth Sci., 57, 3-13, https://doi.org/10.1007/s11430-013-4793-0, 2014.

Wu, Y., Zhang, R., Tian, P., Tao, J., Hsu, S. C., Yan, P., Wang, Q., Cao, J., Zhang, X., and Xia, X.: Effect of ambient humidity on the light absorption amplification of black carbon in Beijing during January 2013, Atmos. Environ., 124, 217-223, https://doi.org/10.1016/j.atmosenv.2015.04.041, 2016.

Wu, Z., Wang, Y., Tan, T., Zhu, Y., Li, M., Shang, D., Wang, H., Lu, K., Guo, S., Zeng, L., and Zhang, Y.: Aerosol Liquid Water Driven by Anthropogenic Inorganic Salts: Implying Its Key Role in Haze Formation over the North China Plain, Environ. Sci. Technol. Lett., 5, 160-166, https://doi.org/10.1021/acs.estlett.8b00021, 2018.

Xie, C., Xu, W., Wang, J., Wang, Q., Liu, D., Tang, G., Chen, P., Du, W., Zhao, J., Zhang, Y., Zhou, W., Han, T., Bian, Q., Li, J., Fu, P., Wang, Z., Ge, X., Allan, J., Coe, H., and Sun, Y.: Vertical characterization of aerosol optical properties and brown carbon in winter in urban Beijing, China, Atmos. Chem. Phys., 19, 165-179, https://doi.org/10.5194/acp-19-165-2019, 2019.

Xing, L., Wu, J., Elser, M., Tong, S., Liu, S., Li, X., Liu, L., Cao, J., Zhou, J., El-Haddad, I., Huang, R., Ge, M., Tie, X., Prévôt, A. S. H., and Li, G.: Wintertime secondary organic aerosol formation in Beijing-Tianjin-Hebei (BTH): contributions of HONO sources and heterogeneous reactions, Atmos. Chem. Phys., 19, 2343-2359, https://doi.org/10.5194/acp-19-2343-2019, 2019.

Xu, L., Liu, L., Zhang, J., Zhang, Y., Ren, Y., Wang, X., and Li, W.: Morphology, Composition,

https://doi.org/10.5194/acp-2019-1025
Preprint. Discussion started: 8 January 2020
© Author(s) 2020. CC BY 4.0 License.

and Mixing State of Individual Aerosol Particles in Northeast China during Wintertime, Atmosphere, 8, 47-57, https://doi.org/10.3390/atmos8030047, 2017.

Xue, J., Yuan, Z., Griffith, S. M., Yu, X., Lau, A. K., and Yu, J. Z.: Sulfate Formation Enhanced by a Cocktail of High NO_x, SO_2, Particulate Matter, and Droplet pH during Haze-Fog Events in Megacities in China: An Observation-Based Modeling Investigation, Environ. Sci. Technol., 50, 7325-7334, https://doi.org/10.1021/acs.est.6b00768, 2016.

Yan, X., Ohara, T., and Akimoto, H.: Bottom-up estimate of biomass burning in mainland China, Atmos. Environ., 40, 5262-5273, https://doi.org/10.1016/j.atmosenv.2006.04.040, 2006.

Yang, T., Gbaguidi, A., Yan, P., Zhang, W., Zhu, L., Yao, X., Wang, Z., and Chen, H.: Model elucidating the sources and formation mechanisms of severe haze pollution over Northeast mega-city cluster in China, Environ. Pollut., 230, 692-700, https://doi.org/10.1016/j.envpol.2017.06.007, 2017.

Zhang, J., Liu, L., Wang, Y., Ren, Y., Wang, X., Shi, Z., Zhang, D., Che, H., Zhao, H., Liu, Y., Niu, H., Chen, J., Zhang, X., Lingaswamy, A. P., Wang, Z., and Li, W.: Chemical composition, source, and process of urban aerosols during winter haze formation in Northeast China, Environ. Pollut., 231, 357-366, https://doi.org/10.1016/j.envpol.2017.07.102, 2017.

Zhang, X., Sun, J., Wang, Y., Li, W., Zhang, Q., Wang, W., Quan, J., Cao, G., Wang, J., and Yang, Y.: Factors contributing to haze and fog in China, Chinese Sci. Bull., 58, 1178-1187, https://doi.org/10.1360/972013-150, 2013.

Zhang, Y., Schauer, J. J., Zhang, Y., Zeng, L., Wei, Y., Liu, Y., and Shao, M.: Characteristics of particulate carbon emissions from real-world Chinese coal combustion, Environ. Sci. Technol., 42, 5068-5073, https://doi.org/10.1021/es7022576, 2008.

Zhang, Y., Yuan, Q., Huang, D., Kong, S., Zhang, J., Wang, X., Lu, C., Shi, Z., Zhang, X., and Sun, Y.: Direct observations of fine primary particles from residential coal burning: insights into their morphology, composition, and hygroscopicity, J. Geophys. Res.-Atmos., 123, 12964-12979, https://doi.org/10.1029/2018JD028988, 2018a.

Zhang, Y., Zhang, Q., Cheng, Y., Su, H., Li, H., Li, M., Zhang, X., Ding, A., and He, K.: Amplification of light absorption of black carbon associated with air pollution, Atmos. Chem. Phys., 18, 9879-9896, https://doi.org/10.5194/acp-18-9879-2018, 2018b.

Zhang, Y. L., Kawamura, K., Agrios, K., Lee, M., Salazar, G., and Szidat, S.: Fossil and Nonfossil Sources of Organic and Elemental Carbon Aerosols in the Outflow from Northeast China, Environ. Sci. Technol., 50, 6284-6292, https://doi.org/10.1021/acs.est.6b00351, 2016.

Zhao, B., Zheng, H., Wang, S., Smith, K. R., Lu, X., Aunan, K., Gu, Y., Wang, Y., Ding, D., Xing, J., Fu, X., Yang, X., Liou, K.-N., and Hao, J.: Change in household fuels dominates the decrease in $PM_{2.5}$ exposure and premature mortality in China in 2005–2015, P. Natl. Acad. Sci. USA, 115, 12401-12406, https://doi.org/10.1073/pnas.1812955115, 2018a.

Zhao, H., Che, H., Xia, X., Wang, Y., Wang, H., Wang, P., Ma, Y., Yang, H., Liu, Y., Wang, Y., Gui, K., Sun, T., Zheng, Y., and Zhang, X.: Multiyear Ground-Based Measurements of Aerosol Optical Properties and Direct Radiative Effect Over Different Surface Types in Northeastern China, J. Geophys. Res.-Atmos., 123, 13887-13916, https://doi.org/10.1029/2018JD029141, 2018b.

Zhao, X. J., Zhao, P. S., Xu, J., Meng, W., Pu, W. W., Dong, F., He, D., and Shi, Q. F.: Analysis of a winter regional haze event and its formation mechanism in the North China Plain, Atmos. Chem.

https://doi.org/10.5194/acp-2019-1025
Preprint. Discussion started: 8 January 2020
© Author(s) 2020. CC BY 4.0 License.

928 Phys., 13, 5685-5696, https://doi.org/10.5194/acp-13-5685-2013, 2013.
929 Zheng, B., Zhang, Q., Zhang, Y., He, K., Wang, K., Zheng, G., Duan, F., Ma, Y., and Kimoto, T.:
930 Heterogeneous chemistry: a mechanism missing in current models to explain secondary inorganic
931 aerosol formation during the January 2013 haze episode in North China, Atmos. Chem. Phys., 15,
932 2031-2049, https://doi.org/10.5194/acp-15-2031-2015, 2015a.
933 Zheng, G. J., Duan, F. K., Su, H., Ma, Y. L., Cheng, Y., Zheng, B., Zhang, Q., Huang, T., Kimoto,
934 T., Chang, D., Pöschl, U., Cheng, Y. F., and He, K. B.: Exploring the severe winter haze in Beijing:
935 the impact of synoptic weather, regional transport and heterogeneous reactions, Atmos. Chem.
936 Phys., 15, 2969-2983, https://doi.org/10.5194/acp-15-2969-2015, 2015b.
937 Zhi, G., Chen, Y., Xue, Z., Meng, F., Cai, J., Sheng, G., and Fu, J.: Comparison of elemental and
938 black carbon measurements during normal and heavy haze periods: implications for research,
939 Environ. Monit. Assess., 186, 6097-6106, https://doi.org/10.1007/s10661-014-3842-2, 2014.
940 Zhong, J., Zhang, X., Wang, Y., Wang, J., Shen, X., Zhang, H., Wang, T., Xie, Z., Liu, C., Zhang,
941 H., Zhao, T., Sun, J., Fan, S., Gao, Z., Li, Y., and Wang, L.: The two-way feedback mechanism
942 between unfavorable meteorological conditions and cumulative aerosol pollution in various haze
943 regions of China, Atmos. Chem. Phys., 19, 3287-3306, https://doi.org/10.5194/acp-19-3287-2019,
944 2019.
945 Zou, J., Wang, M., Zhao, S., Wu, X., Zhao, L., Liu, J., Gao, W., Tang, G., Xin, J., Wang, L., Ji, D.,
946 Xu, H., Wang, Y., and Hu, B.: Case study of the effects of aerosol chemical composition and
947 hygroscopicity on the scattering coefficient in summer, Xianghe, southeast of Beijing, China,
948 Atmos. Res., 225, 81-87, https://doi.org/10.1016/j.atmosres.2019.03.026, 2019.

949

https://doi.org/10.5194/acp-2019-1025
Preprint. Discussion started: 8 January 2020
© Author(s) 2020. CC BY 4.0 License.

Atmospheric Chemistry and Physics Discussions

Figure Captions

Figure 1. (a) Topographic features of Northeast China, which is surrounded by the Greater Khingan Mountains, the Lesser Khingan Mountains, and the Changbai Mountains. **(b)** Locations of the urban and mountain sites. The relief map in panel (a) is from OpenStreetMap contributors 2019 distributed under a Creative Commons BY-SA License (https://maps-for-free.com/).

Figure 2. Variation in the concentrations of $PM_{2.5}$, organic matter (OM), elemental carbon (EC), and water-soluble ions (i.e., Ca^{2+}, Mg^{2+}, K^+, Na^+, NH_4^+, NO_3^-, SO_4^{2-}, Cl^-, and F^-) at the urban and mountain sites from daytime (DT) on 31 October to nighttime (NT) on 5 November 2016: **(a)** $PM_{2.5}$; **(b-c)** OM, EC, and water-soluble ions. Two regional haze episodes (Haze-I: 31 NT October-4 DT November; Haze-II: 4 NT-5 NT November) were identified.

Figure 3. Typical transmission electron microscopy (TEM) images and energy-dispersive X-ray spectrometry (EDS) spectra of different types of individual aerosol particles: **(a)** mineral particle; **(b)** spherical OM particle; **(c)** domelike OM particle; **(d)** soot particle; **(e)** Fe-rich particle; **(f)** mixture of S-rich and OM particles; **(g)** mixture of soot, S-rich, and OM particles; **(h)** mixture of Fe-rich and S-rich particles; **(i-j)** mixture of K-rich and OM particles at the urban and mountain sites. The EDS spectra of these particle components are located below their TEM images. **(k)** a typically spherical OM particle and its NanoSIMS ion intensity mappings of $^{12}C^{14}N^-$, $^{12}C^-$, $^{16}O^-$, and $^{32}S^-$ signals.

Figure 4. Variation in number fractions of different types of particles at the urban and mountain sites. Analyzed particle numbers are listed on the top of each rectangle.

Figure 5. Variation in $PM_{2.5}$/EC, OC/EC, SO_4^{2-}/EC, NO_3^-/EC, and K^+/EC factors at the urban site **(a)** and mountain site **(b)**. These factors are normalized.

Figure 6. Typical TEM images of individual aerosol particles at low magnification at the urban and mountain sites: **(a-b)** clean day; **(c-d)** Haze-I; **(e-f)** Haze-II.

Figure 7. Linear correlations between $PM_{2.5}$ mass concentration (x) and K-OM

https://doi.org/10.5194/acp-2019-1025
Preprint. Discussion started: 8 January 2020
© Author(s) 2020. CC BY 4.0 License.

Atmospheric Chemistry and Physics Discussions

978 number fraction (y) during the Haze-I **(a)** and Haze-II **(b)**. Typical 24-h air mass
979 backward trajectories before arriving at the urban and mountain sites during the Haze-I
980 **(c)** and Haze-II **(d)**. Fire spot data are from the MODIS Collection 6 Active Fire
981 Product provided by the NASA FIRMS (https://firms.modaps.eosdis.nasa.gov/map/).
982 **Figure 8.** Schematic diagram of Haze-I and Haze-II formation in Northeast China
983 during winter. The major emission sources and haze formation processes are shown.

https://doi.org/10.5194/acp-2019-1025
Preprint. Discussion started: 8 January 2020
© Author(s) 2020. CC BY 4.0 License.

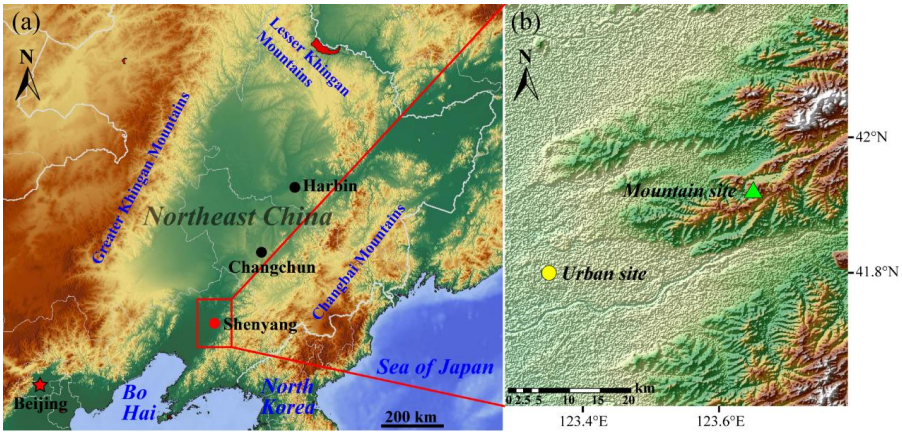

Figure 1.

https://doi.org/10.5194/acp-2019-1025
Preprint. Discussion started: 8 January 2020
© Author(s) 2020. CC BY 4.0 License.

Atmospheric Chemistry and Physics Discussions

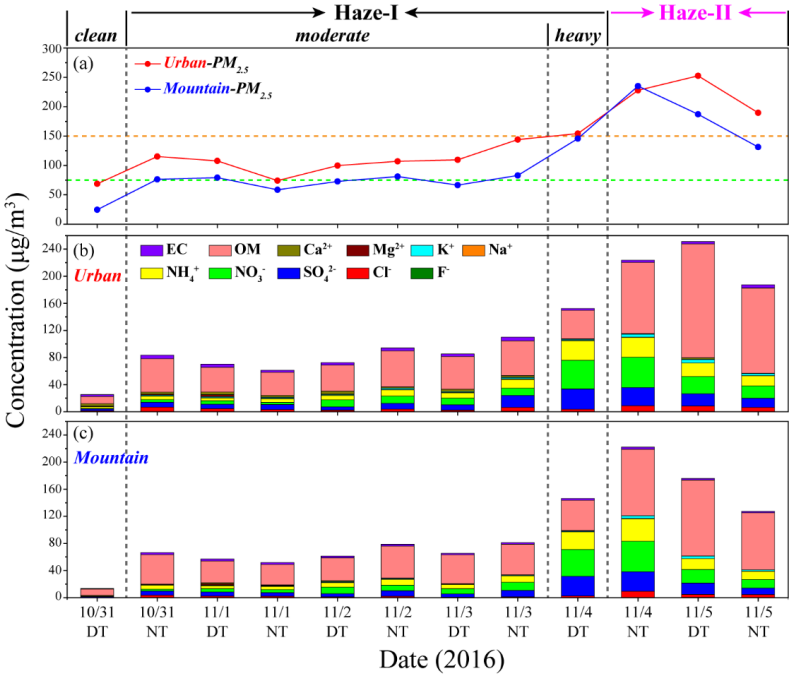

986

987 **Figure 2.**

https://doi.org/10.5194/acp-2019-1025
Preprint. Discussion started: 8 January 2020
© Author(s) 2020. CC BY 4.0 License.

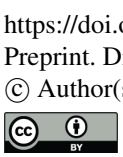

Atmospheric Chemistry and Physics Discussions

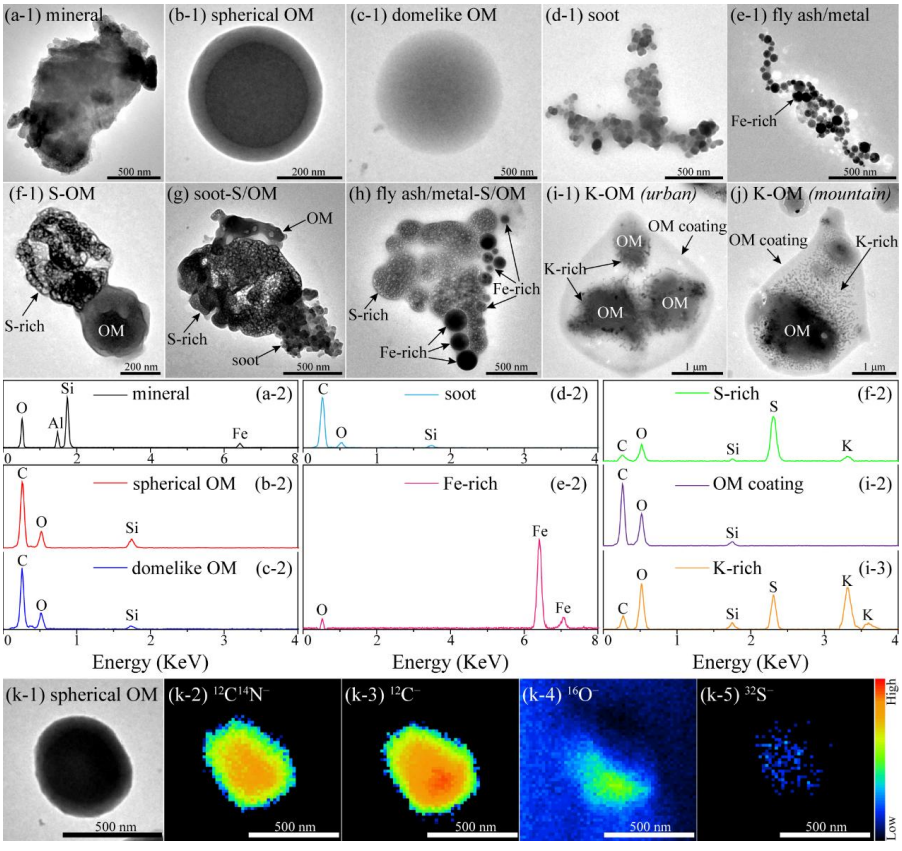

Figure 3.

https://doi.org/10.5194/acp-2019-1025
Preprint. Discussion started: 8 January 2020
© Author(s) 2020. CC BY 4.0 License.

Atmospheric Chemistry and Physics Discussions

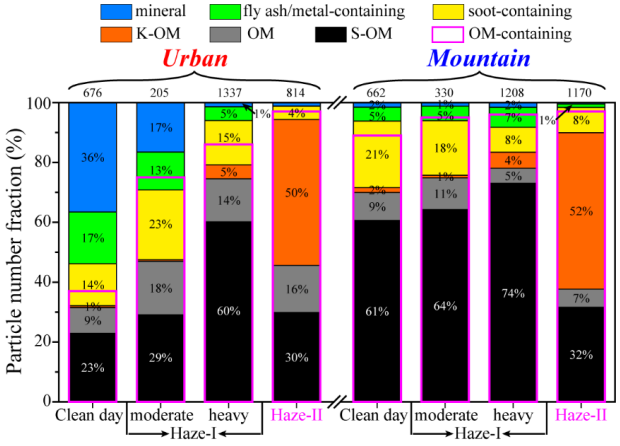

990

991 **Figure 4.**

https://doi.org/10.5194/acp-2019-1025
Preprint. Discussion started: 8 January 2020
© Author(s) 2020. CC BY 4.0 License.

Atmospheric Chemistry and Physics Discussions

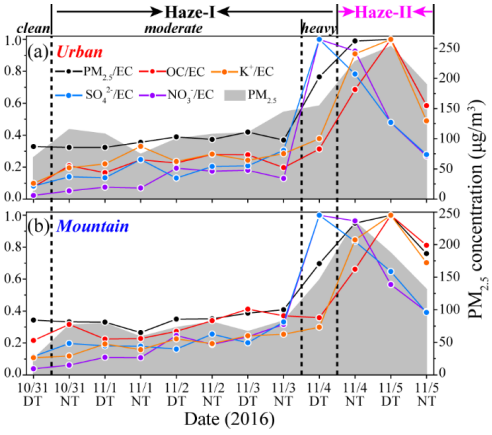

992

993 **Figure 5.**

https://doi.org/10.5194/acp-2019-1025
Preprint. Discussion started: 8 January 2020
© Author(s) 2020. CC BY 4.0 License.

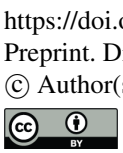

Atmospheric Chemistry and Physics Discussions

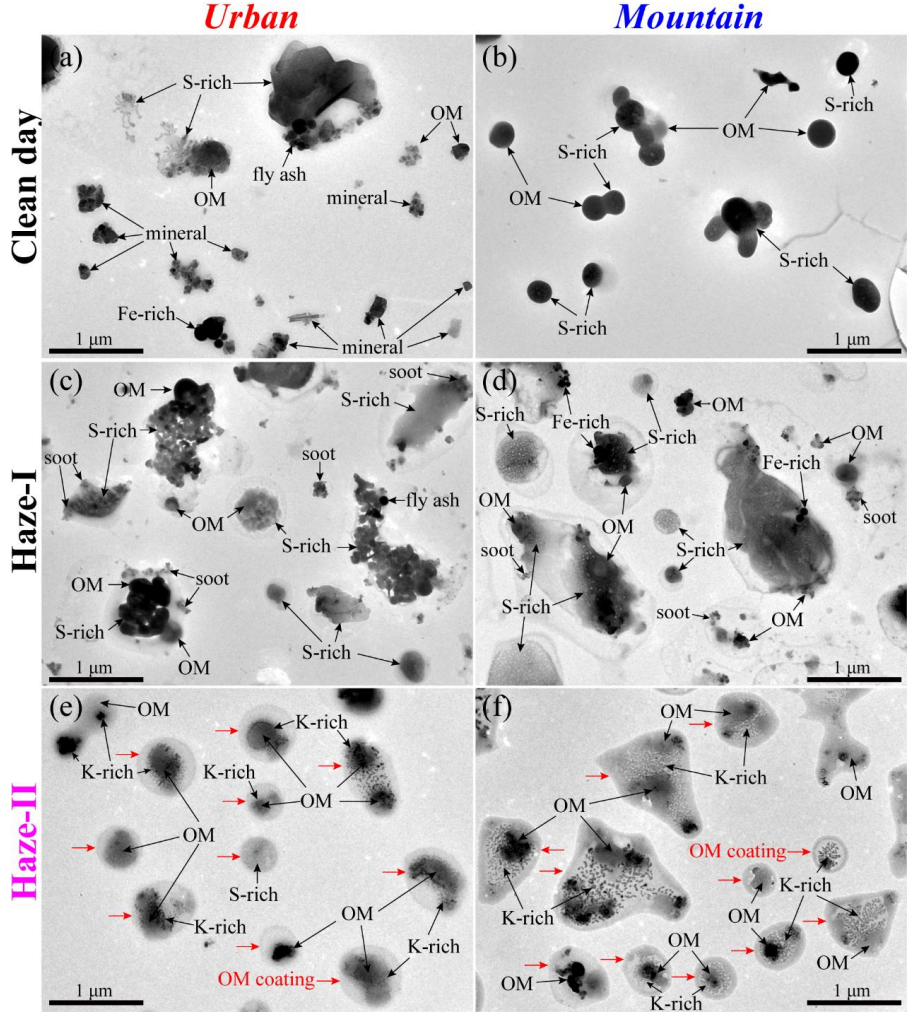

Figure 6.

https://doi.org/10.5194/acp-2019-1025
Preprint. Discussion started: 8 January 2020
© Author(s) 2020. CC BY 4.0 License.

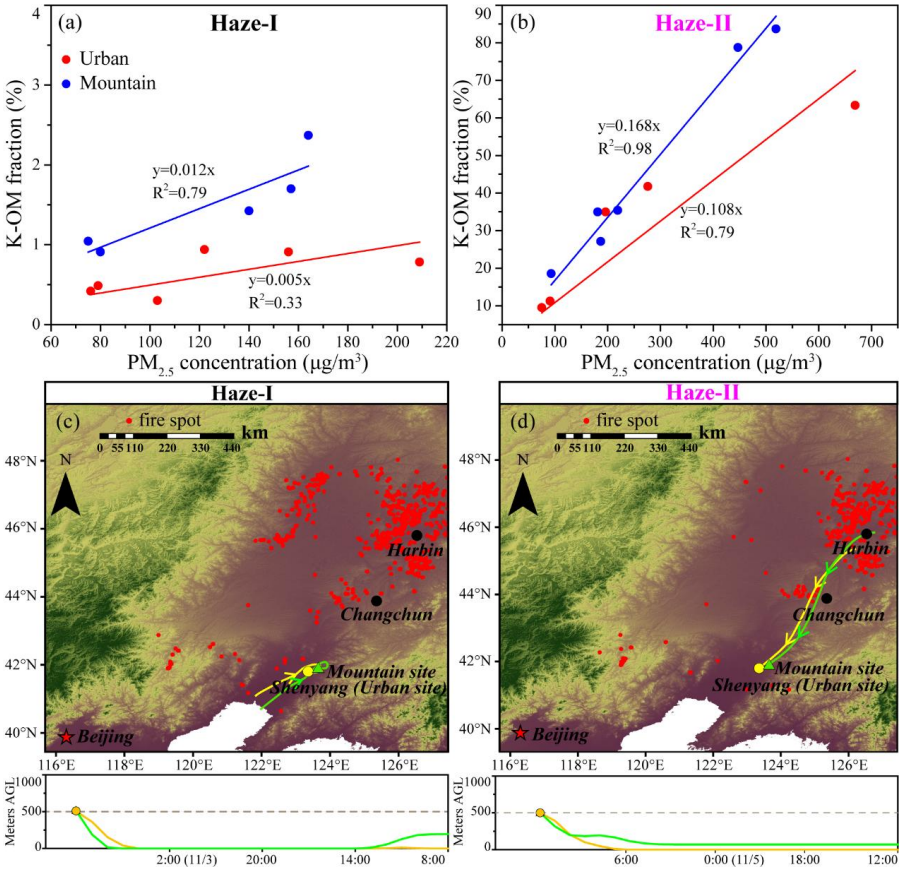

Figure 7.

https://doi.org/10.5194/acp-2019-1025
Preprint. Discussion started: 8 January 2020
© Author(s) 2020. CC BY 4.0 License.

Atmospheric Chemistry and Physics Discussions

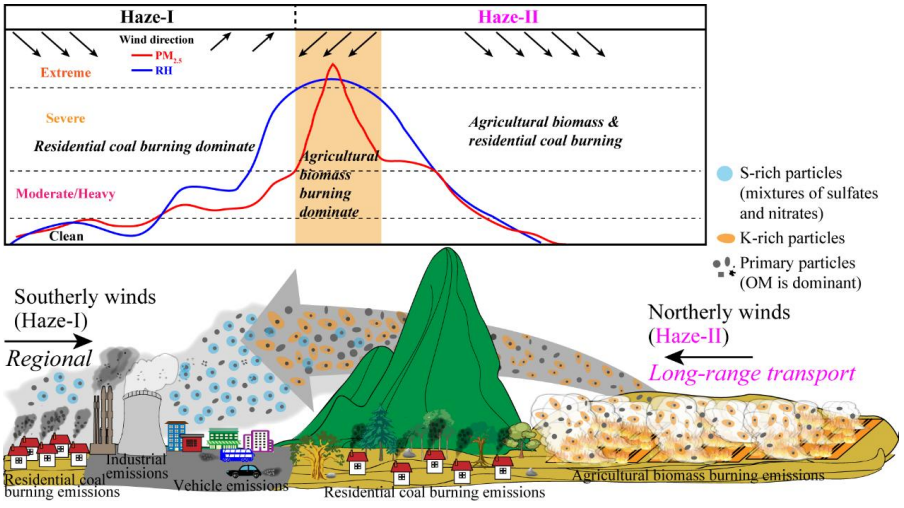

998

999 **Figure 8.**